AFIT/GEP/ENP/92D-06

CATION PRODUCTION AND REACTIONS INDUCED BY ELECTRON IMPACT ON TETRAETHOXYSILANE

THESIS

Jeremy C. Holtgrave
First Lieutenant, USAF

AFIT/GEP/ENP/92D-06

Approved for public release; distribution unlimited

AFIT/GEP/ENP/92D-06

CATION PRODUCTION AND REACTIONS INDUCED BY ELECTRON IMPACT ON TETRAETHOXYSILANE

THESIS

Presented to the Faculty of the School of Engineering

of the Air Force Institute of Technology

Air University

In Partial Fulfillment of the

Requirements for the Degree of

Master of Science in Engineering Physics

Jeremy C. Holtgrave, B.S.

First Lieutenant, USAF

December, 1992

Preface

The purpose of this project was to examine the positive ion species produced when gaseous tetraethoxysilane (TEOS, $Si(OC_2H_5)_4$) was impacted by electrons and to investigate the subsequent ion chemistry. TEOS is currently being evaluated by the scientific community as a possible replacement for silane in the plasma enhanced chemical vapor depostion of silicon dioxide dielectric films. The primary tool used in this investigation was a Fourier Transform mass spectrometer provided by the Advanced Plasma Research group (WL/POOC-3). It offered the benefits of high mass resolution and the ability to examine the ion chemistry *in situ.*

In retrospect I see this project was an enormous undertaking and I owe thanks to all who helped me along the way. In particular, I would like to thank Dr. Peter Haaland, my advisor, for his guidance, patience and most of all for the confidence he expressed in my work. He provided a base of knowledge and experience I lacked and he kept me on track as I delved into the details of the experiment. Also, I would like the thank Dr. Alan Garscadden (WL/POOC-3) for agreeing to serve on my thesis committee. His comments, suggestions, and insights, were very much appreciated. And finally, I am deeply indebted to Major Kevin Riehl for showing me the nuts and bolts of FTMS. Throughout the summer and fall he went far out of his way to get me started in the lab and to explain the operating principles of FTMS. This thesis would not have happened without him.

Jeremy C. Holtgrave

Table of Contents

List of Figures

List of Tables

Abstract

The production of cations by electron impact on tetraethoxysilane (TEOS) is studied with a Fourier Transform mass spectrometer (FTMS). The operating principles of FTMS are reviewed and the experimental approach to the mass calibration and cross-section measurement is discussed. The cross-sections for total and partial ionization of $Si(OC_2H_5)_4$ from threshold to 50 eV are measured. Also, the ion chemistry resulting from interactions between ions and neutral TEOS is examined.

CATION PRODUCTION AND REACTIONS INDUCED BY ELECTRON IMPACT ON TETRAETHOXYSILANE

I. Introduction

1.1 Overview

The deposition of SiO_2 as a thin dielectric film is a key aspect of current semiconductor technology. While thermal chemical vapor deposition is still widely used for this application, plasma enhanced chemical vapor deposition (PECVD) is used as well. Current PECVD reactors use silane (SiH_4) and oxygen (O_2) as reactants, however, some of the deposition characteristics provided by silane are undesirable [2:1]. Tetraethoxysilane (TEOS, $Si(OC_2H_5)_4$) has recently been investigated as a possible replacement. While experiments have been conducted to determine the suitability of TEOS as a silicon source, the TEOS/O_2 plasma itself is not well understood. The purpose of this work is to examine the production of ions by electron impact on TEOS and characterize how these ions react chemically in a plasma.

1.2 Approach/Objective

The overlying approach was to use Fourier Transform Mass Spectrometry (FTMS) to characterize the creation of ions when gaseous TEOS was bombarded with electrons. The first objective was to identify as precisely as possible the ions created. The second step then was to measure the partial ionization cross-sections of these ions. Finally, the third objective was to examine the chemistry of these ions as they reacted with the neutral TEOS background. Fourier Transform mass spectrometry was ideally suited to investigate this problem for several reasons. First,

the ions could be identified on the spot without having to sweep them into another instrument. Secondly, this spectrum could be obtained with more than the unit mass resolution obtained by other instruments. And finally, the entire spectrum could be acquired simultaneously without having to sweep through a range of mass channels.

1.3 Background

Studies on the use of TEOS as a silicon source in the depostion of thin films have been conducted since the early sixties [14, 19, 7, 1, 5, 18, 10, 3, 9, 13, 17, 8]. For the most part these works have concentrated on determining the quality of the SiO_2 films produced by TEOS/O_2 plasmas in various reactors.

The TEOS/O_2 plasma itself was investigated recently by Charles *et. al.* [2]. This work specifically investigated neutral species impinging on the reactor walls for a pure TEOS plasma and a TEOS/O_2 plasma. While this is a step towards understanding the surface chemistry involved in creating thin films, the issue of the production of ions in the plasma and their role in the deposition process is still unresolved. The goal of this thesis is to address this question by examining the production of positive ions by electron impact and observe how these ions react after production.

II. Experimental Approach

This chapter outlines theoretical aspects of FTMS as they pertain to the measurement of ionization cross-sections and ion-molecule reactions.

2.1 FTMS Principles

FTMS is based on cyclotron resonance theory. Ions are created by electron impact in a cubic trap immersed in a uniform magnetic field. A sinusoidal potential ($V_e(t)$) is applied to two opposite cube sides parallel to the magnetic field (excite plates) as shown in Figure 2.1. If this potential is made to oscillate at the resonance frequency of the ions, they will spiral in a plane perpendicular to the magnetic field. These circling charged particles produce an image current (with an associated voltage $V_s(t)$) at the ion's resonant frequency on the other two sides parallel to the magnetic field (detect plates) [4:4097]. The remaining two sides (trapping plates) are normally placed at a constant potential (V_t) to keep the ions trapped in the axial direction. Note that if the trapping plates are held at a positive voltage then cations are trapped and anions ejected. If they are held at a negative voltage then anions are trapped and cations ejected.

2.1.1 Ion Trap Theory The formula for ion cyclotron resonance is:

$$f_c = \frac{qB}{2\pi m} \tag{2.1}$$

where f_c is the frequency of oscillation, q and m are the ion's charge and mass, and B is the magnetic field strength. For singly charged ions the mass is inferred from the observed cyclotron frequency.

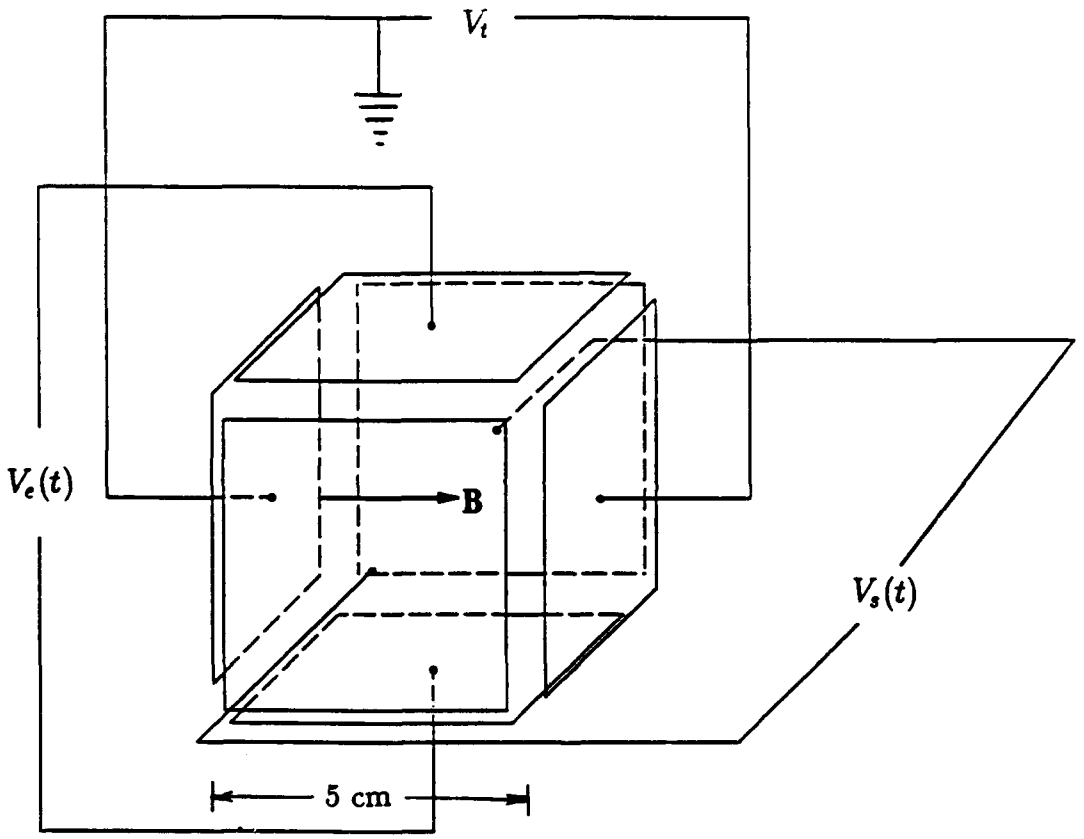

Figure 2.1. Ion Trap Configuration. The ions spiral in the plane perpendicular to the magnetic field. $V_e(t)$ is the excitation potential, $V_s(t)$ is the potential associated with the image current, and V_t is the trapping voltage.

The ions are excited into cyclotron motion by an electric field applied between the excite plates. For large excite plates driven by an applied voltage:

$$V_e(t) = V_{0e} \sin(2\pi f_c t) \tag{2.2}$$

the cyclotron radius is increased at a constant rate according to:

$$r(t) = \frac{V_{0e} t}{2aB} \tag{2.3}$$

where a is the distance between the plates [4:4101]. If the excitation is turned off at some time t_0, the ions will continue to orbit at a radius $r(t_0)$. Since this quantity is independent of mass, all ion species can be excited coherently to a single radius. This turns out to be a necessary condition for a meaningful analysis of the image current.

The orbiting ions then induce an image current on the detect plates. Coherent excitation and capacitive detection yields:

$$V_s(t) = \frac{Nqr(t_0)}{aC} \sin(2\pi f_c t - \frac{\pi}{2}) \tag{2.4}$$

where V_s is the voltage signal induced by the rotating charge, N is the number of charges, and C is the capacitance of the detector circuit [4]. Substituting Eq (2.3) into Eq (2.4) gives:

$$V_{0s} = \frac{NqV_{0e}t_0}{2a^2BC} \tag{2.5}$$

where V_{0s} is the amplitude of the induced voltage. This equation is still independent of mass and is linear in the number of charges as well as the charge itself. This means it is possible to excite a collection of molecules with the same ionization state but different masses to the same radius and measure a voltage signal directly proportional to the number of ions in the trap. This feature of FTMS allows one to infer the number of ions in the trap directly from the amplitude of the signal voltage.

Up to now FTMS theory has been developed assuming ideal conditions. The cyclotron resonance equation assumes no stray electric fields, the radius equation assumes infinite parallel excite plates, and the equation governing the signal voltage assumes infinite parallel detect plates. But for a collection of ions in a cubic trap, these assumptions are not quite true.

Trapping plates and space charge produce electric field components perpendicular to the magnetic field and perturb the cyclotron frequency. This perturbation was examined in detail by Ledford, *et. al.* [11] who found that the relation between ion mass and frequency is more precisely:

$$m_i^2 f_i^2 = a_0 + b_0 m_i + c_0 m_i^2 \tag{2.6}$$

where m_i is the mass of the ith species, f_i is the oscillation frequency of the ith species, and a_0, b_0, and c_0 are adjustable parameters which depend on the ionic charge, and the trapping geometry. These parameters are independent of mass and can be determined empirically by taking a spectrum of known masses and applying Eq (2.6). Once a_0, b_0, and c_0 are known the transformation from frequency to mass is:

$$m_i = \frac{-b_0 \pm \sqrt{b_0^2 - 4a_0(c_0 - f_i^2)}}{2(c_0 - f_i^2)} \tag{2.7}$$

While this is a more complicated transformation than can be derived from Eq (2.1), it begins to account for the real physics of the ion trap and is necessary for the high mass resolution.

Another realistic consideration is the fact that the excite and detect plates are not infinitely large. In order to predict the motion of the ions it is necessary to accurately model the time varying potential for a finite cubic trap. With this the ion trajectory can be calculated along with the image current it induces. This matter was examined in detail by Riehl [16]. He found that although Eq (2.5) is only a first order approximation, the linear relation between signal and ion number holds.

As was mentioned previously, ions are created by electron impact. Electrons are shot into the trap along the magnetic field axis and collected in a Faraday cup. The beam must be aligned very carefully with the magnetic field or the electrons will be deflected away from the cup. Also, as they enter the trap and traverse the axial direction, they experience the trapping potential and undergo shifts in the energy accordingly. It is not possible to know exactly what energy each electron had when it created each ion. It is possible to calculate the average energy the electrons had on their way through the trap. This calculation was performed as part of the computational model of the ion trap done by Riehl [15]. His results suggest that if the trapping potential is maintained at 2 Volts then the average electron energy is 1.1 ± 0.4 eV above the incoming beam energy.

2.1.2 Fourier Transform Applications At the heart of this experiment is the Fourier Transform. Since the composition of ions in the trap is unknown at the start, it is necessary to excite a wide range of frequencies simultaneously with the intent of influencing all the ions. This is accomplished with stored waveform inverse Fourier Transform (SWIFT) excitation [6]. The SWIFT waveform in the time domain is shown in Figure 2.2.

The SWIFT excitation in the frequency and mass domain is obtained by taking the Fourier Transform of this and is shown in Figure 2.3. This particular waveform was created to excite masses across a 2 MHz bandwidth corresponding to a range of masses from 10 to 500 a.m.u. All ions within this mass range are excited equally and the Fourier Transform is a plateau across this range.

Once the ions are resonating they deliver a signal current to the detect plates. This signal current will contain frequency components specific to the masses of each ion type. Also, the amplitude of the signal current produced by one particular species is proportional to its abundance in the trap. Therefore, the Fourier Transform of the

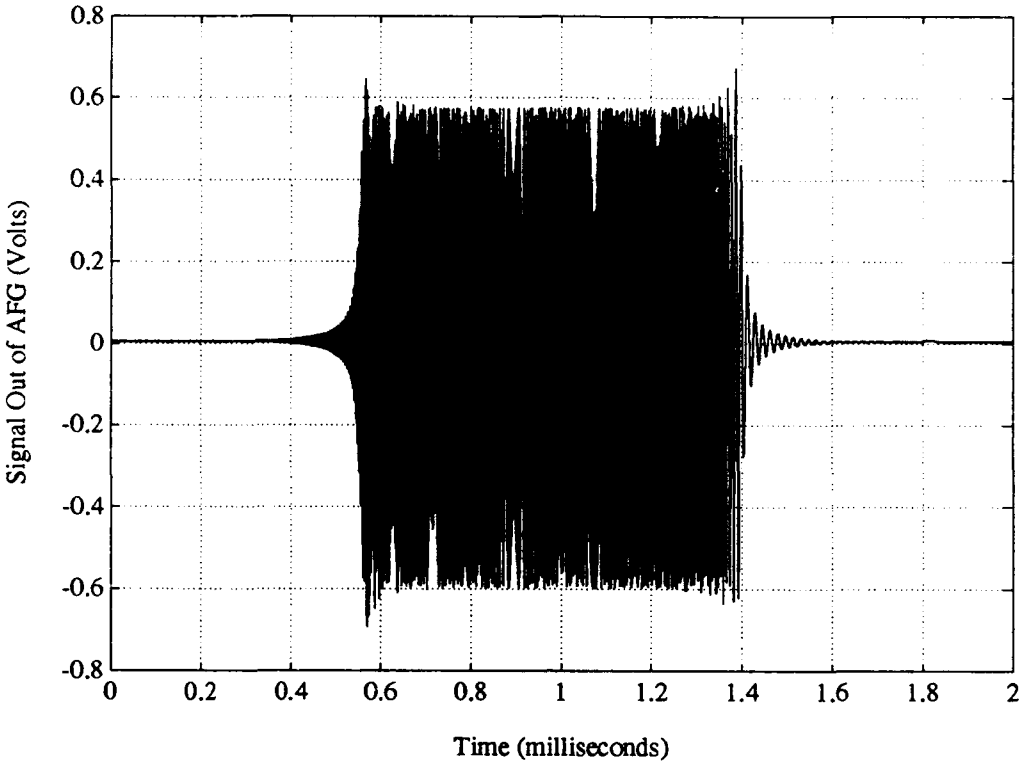

Figure 2.2. SWIFT Excitation Waveform. This is the time domain SWIFT waveform as it plays out of the AFG.

image current yields a mass spectrum along the x axis and the relative concentration of each species along the y axis.

2.2 Ionization and Ion Kinetics

The physical process studied is the creation of ions by electron impact on TEOS and their subsequent chemical behavior.

$$TEOS + e \rightarrow A^{+} + B + 2e \tag{2.8}$$

Since $TEOS$ is a large molecule with 33 constituant atoms one expects to observe a variety of products for A^{+}. For each product A^{+} there is an associated partial

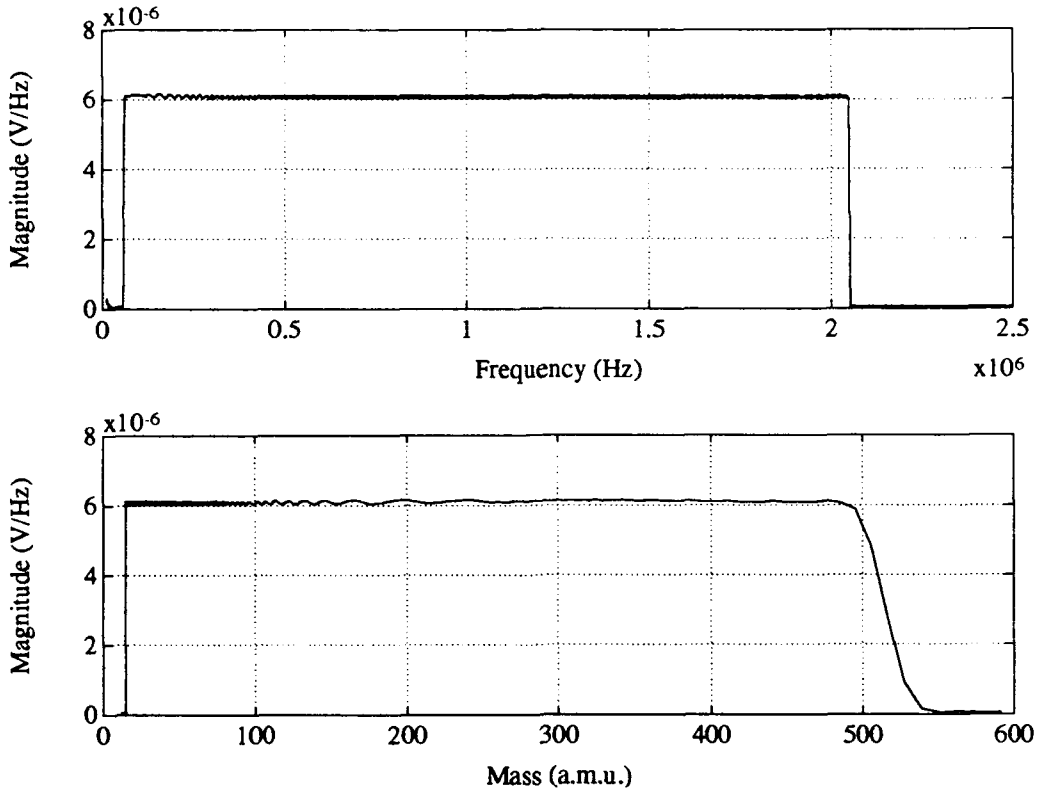

Figure 2.3. SWIFT Excitation Spectrum. The Fourier Transform of Figure 2.2 gives the excitation spectrum in the frequency domain (upper plot) and in the mass domain (lower plot).

ionization cross-section. The high mass resolution of FTMS allows one to observe A^+ unambiguously while the linear dependence of peak intensity in the frequency domain to the number of ions in the trap allows one to measure the partial ionization cross-section. By varying the electron energy, then, one can map this cross-section over some convenient range. Note that Eq (2.8) is not the only possible result of an electron impacting on TEOS. For example,

$$TEOS + e \rightarrow A^+ + B^+ + 3e \tag{2.9}$$

is possible as well. But this process requires more energy and since this work examines energies just above the ionization threshold, Eq (2.8) is assumed to be the dominant process.

The partial ionization cross-section for each product A^+ can be obtained from the data by the following relation:

$$\frac{dn^+}{dt} = nn_e\langle\sigma v\rangle \tag{2.10}$$

where n and n_e are the concentrations of the TEOS vapor and electrons, v is the relative velocity between the two, and σ is the partial ionization cross-section for the positive ion n^+. If one multiplies through by the time differential dt and assumes all the electrons have the same velocity relative to the ions then this expression reduces to:

$$dn^+ = nn_e\sigma dx \tag{2.11}$$

where dx is some arbitrary length element within the trap. If n_e is the concentration of electrons in the trap then $n_e dx = \frac{N_e}{A}$ where N_e is the total number of electrons put through the trap and A is the area through which they traveled. Since each electron has charge $-e$, N_e can be replaced with $\frac{Q_{tot}}{e}$ giving:

$$n_e = \frac{Q_{tot}}{eA} \tag{2.12}$$

The concentration of TEOS can be obtained by rearranging the Ideal Gas Law:

$$n = \frac{P}{RT} \tag{2.13}$$

where P is the TEOS vapor pressure, R is the universal gas constant, and T is the vapor temperature. As explained previously, the number of ions created in the trap dn^+ is directly proportional to the intensity I_+ of the n^+ peak in the mass domain.

Stating this mathematically:

$$dn^+ = CI_{n+} \tag{2.14}$$

where C is the proportionality constant. Plugging all this into Eq (2.11) and solving for σ gives:

$$\sigma = \frac{eARTCI_{n+}}{PQ_{tot}} \tag{2.15}$$

For this experiment A, T, and K are not known. However, those numbers are assumed to be the same no matter what gas is in the ion trap. If one performs the same experiment on a reference gas of known cross-section then the quantity $(eARTC)$ can be measured empirically and substituted into Eq (2.15). This gives:

$$\frac{\sigma PQ_{tot}}{I_{n+}} = \frac{\sigma_0 P_0 Q_{0tot}}{I_{0n+}} \tag{2.16}$$

where the subscript "$_0$" refers the same quantities defined above as applicable to the reference gas.

With the cross-section data it is then possible to compute the production rates for various species by the relation:

$$k = N_e \int F(\epsilon)\sqrt{\frac{\epsilon}{\mu}}\sigma(\epsilon)d\epsilon \tag{2.17}$$

where k is the production rate, N_e is the electron concentration, ϵ is the electron energy, μ is the reduced mass of the electron-molecule system, $\sigma(\epsilon)$ is the cross-section, and $F(\epsilon)$ is assumed to be a Maxwellian energy distribution.

Once the ions are formed one can delay the time between ion creation and ion observation. This delay allows the ions to react chemically and form new species. That is:

$$A^+ + B \rightarrow C^+ + D \tag{2.18}$$

If the delay time is varied one can observe the time evolution of the ionic species A^+ and C^+. Some species will be consumed, some will be consumed and produced, and others will just be produced. Again, the linear dependence of peak intensity to the number of ions in the trap allows one to observe the growth or decay of the various species as a function of delay time.

If one particular ionic species is observed to be consumed in time, it is possible to calculate the rate constant for that reaction as long as the pressure is known. Consider the differential equation describing the decay of n^+ as it reacts with a neutral species n according to a rate K:

$$\frac{dn^+}{dt} = -n^+ nK \tag{2.19}$$

This differential equation can be solved for n^+ giving:

$$n^+ = Ce^{-nKt} \tag{2.20}$$

where C is a constant determined by the initial conditions. The time constant τ is then related to nK by:

$$\frac{1}{\tau} = nK \tag{2.21}$$

Solving for K gives:

$$K = \frac{1}{n\tau} \tag{2.22}$$

The time constant τ can be read directly from the data and the concentration n can be obtained from the Ideal Gas Law. The final expression is then:

$$K = \frac{kT}{P\tau} \tag{2.23}$$

where T is the temperature (assumed to be room temperature), P is the known pressure, and k is Boltzmann's Constant.

III. Experimental Procedure

This chapter details the data acquisition process and defines the parameters involved with the cross-section and ion chemistry experiments. While some of the important experimental equipment is discussed here, a detailed list can be found in Appendix A of [16].

3.1 Data Acquisition

Acquiring a mass spectrum was conducted in three parts. First, the ions were created, then they were excited, and finally the image current was detected. In order to maintain the ions in a single coherent packet, the trap was kept at pressures on the order of 10^{-7} Torr. This reduced the number of particle collisions which caused the ions to dephase and be ejected from the trap. The three parts associated with taking a mass spectrum are detailed in this section along with a discussion of the parameters applicable to each.

3.1.1 The Digital to Analog Converter The entire FTMS data acquisition run was governed by the Digital to Analog Coverter (DAC). This device has a simultaneous four-channel output producing preprogrammed electronic pulses on a 1 ms time base. The first two channels were used to clear the trap and control the trapping voltage as shown on Figure 3.1. The third was used to control the electron gun and the fourth was used to trigger the SWIFT excitation as shown in Figure 3.2. The SWIFT waveform was played out of an Arbitrary Function Generator (AFG) and the oscilloscopes were triggered off a small pulse encoded at the end of the SWIFT 200 μs after the primary exictation. The ten ms delay between ion creation and excitation assured cutoff of the electron beam.

The entire sequence was repeated every 200 ms yielding a single transient ion signal each time. Typically between 200 to 1000 such transients were collected and

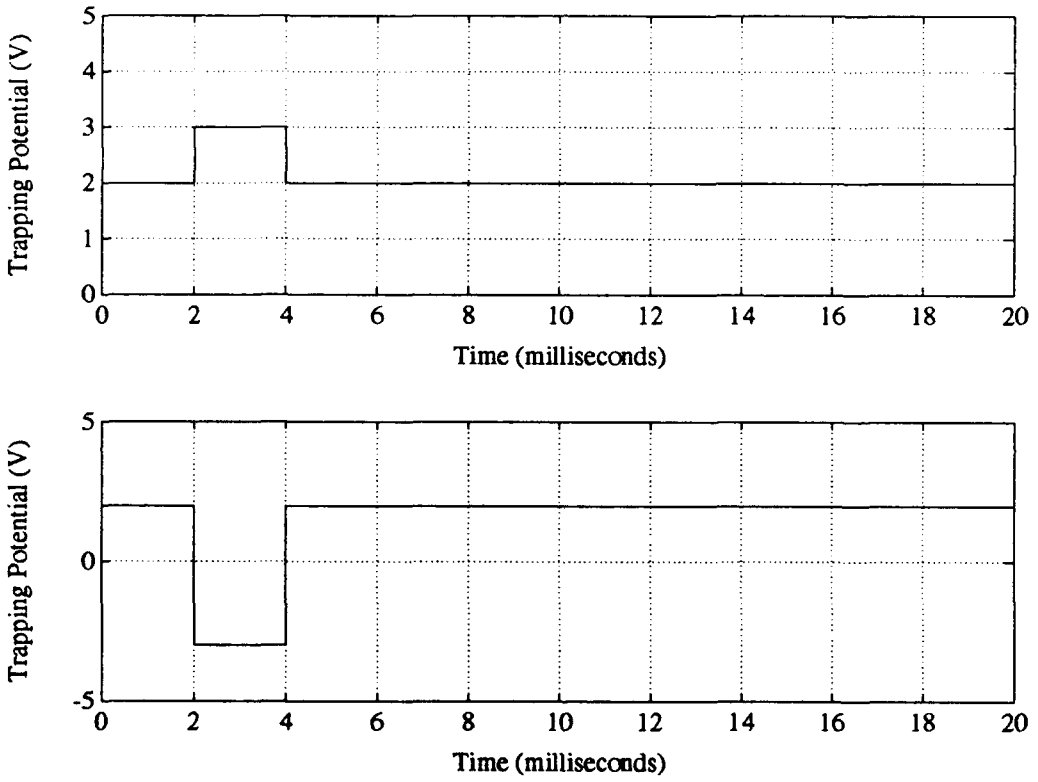

Figure 3.1. DAC Channels One and Two. The first two DAC channels were used to clear the trap of ions and maintain the trapping potential.

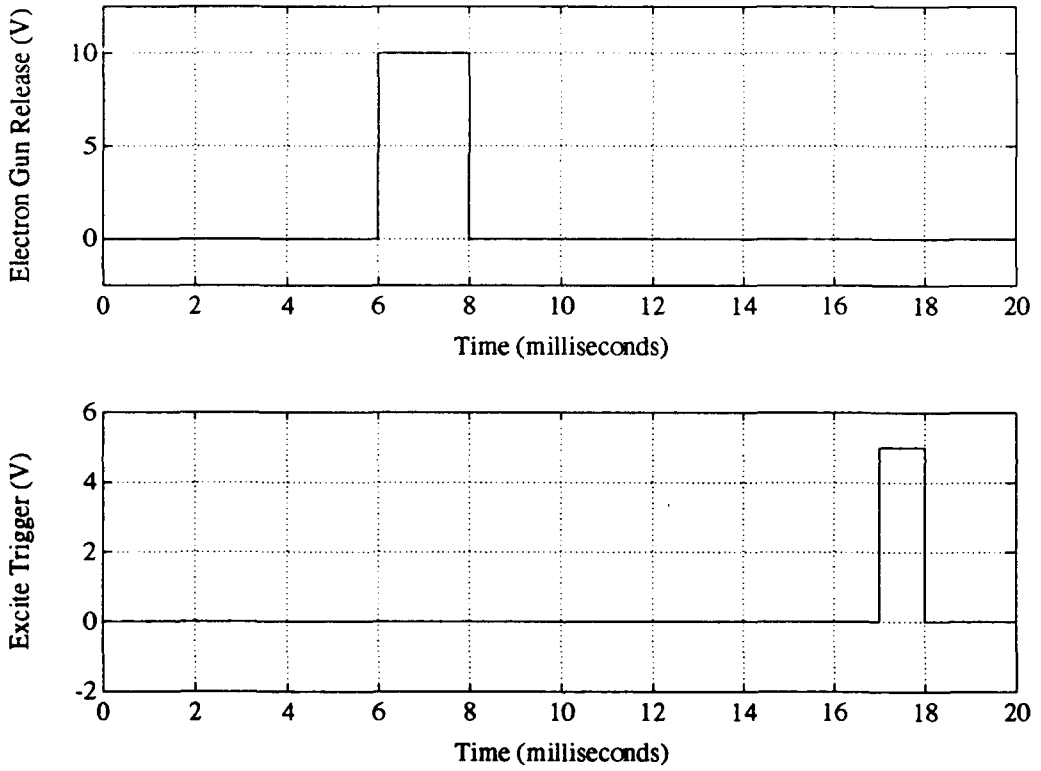

Figure 3.2. DAC Channels Three and Four. Channel three (the upper plot) was used to fire the electron gun and channel four (the lower plot) was used to trigger the excite sequence.

sum averaged. The purpose of this approach was to average out random noise in the signal thereby improving the signal-to-noise ratio.

3.1.2 SWIFT Excitation and the Arbitrary Function Generator The SWIFT excitation was produced by the arbitrary function generator (AFG). Since the AFG is a digital device, sampling became an issue. It was important to make sure the SWIFT excitation clocked out of the AFG in time steps small enough that the ions perceived it as a continuous waveform. If this was not the case the effieciency with which the ions absorbed the excitation was diminished. Also the SWIFT excitation had to be limited to an acceptable amplitude. This amplitude governs the final radius achieved by the orbiting ions which in turn produce the signal current. The final radius had to be large enough that an acceptable image current was induced on the detect plates, but not so large that the ions experienced the distortions in the applied electric field near the plates. Previous work with this apparatus performed by Riehl [16:13–20] addressed both issues and suggested that a SWIFT executed in 50 ns time steps with an amplitude of 700 mV would be efficiently absorbed by the ions and place them in orbits at a radius of 0.96±0.07 cm.

3.1.3 Signal Detection The image current was read as discrete data points by an analog to digital converter (an 8 bit oscilloscope). The parameters used in observing the signal were governed by the sampling theorem and the uncertainty relation. The sampling theorem states that when time domain data is acquired as discrete samples, the maximum frequency observable f_{max} is given by:

$$f_{max} = \frac{1}{2\Delta t} \tag{3.1}$$

where Δt is the time step between samples. This is formally known as the Nyquist frequency. While this places an upper bound on the observable frequency it places a lower bound on the observable mass since the two are inversly related. The uncer-

tainty relation states that the minimum frequency uncertainty Δf associated with an observation is:

$$\Delta f = \frac{1}{2\Delta T} \tag{3.2}$$

where ΔT is the total observation time.

For the oscilloscope used in this experiment the observation time could be made almost arbitrarily long. However, at most 200,000 data points could be recorded. The observation time and number of samples taken were varied in order to suit the needs of each experiment.

3.2 TEOS Measurement Procedure

Once the data acquisition process was understood, carrying out the thesis experiment itself was straightforward. For the mass calibration and the high resolution work it was decided that a 2 MHz Nyquist frequency was acceptable. This meant that with 200,000 data points the system could be observed for 50 ms while cutting off the mass spectrum at 15.2 a.m.u. This allowed the observation of water vapor, the lowest mass ion of interest. Ions lighter than this would consist of simple carbon-hydrogen chains and the trade off of frequency resolution for a broader mass spectrum was unacceptable.

3.2.1 Pulse Valve Pressure Calibration In order to determine the partial ionization cross-sections from the spectral data it was necessary to know both the number of electrons put through the trap and the trap pressure. A Faraday cup placed to receive the electrons was used to measure the beam current. The integral of the beam current gives the beam charge, which is in direct proportion to the number of electrons. Knowing the pressure required the use of the pulse valve and spinning rotor pressure gauge.

The pulse valve is an electronically driven inlet capable of opening and closing at very precise moments in time repeatedly. This allowed exact quantities of gas to

be puffed into the ion trap. The spinning rotor gauge, then, was used to measure the increase in trap pressure caused by the puff. The pressure per puff was determined by closing the gate valve, puffing gas into the system, and recording the change in pressure. Note that once the vacuum system was isolated from chamber there was a finite leakup of gas superimposed on the pulse valve readings. This leakup rate was measured by simply closing the gate valve and taking regular pressure measurements without puffing gas into the trap. It was then used to correct the pulse valve data.

Once the pressure per puff was measured, it was possible to take spectra at known pressures. The ion trap was isolated from the vacuum pump and a particular number of gas puffs was injected into the system. Then the typical spectral acquisition routine was run. It was important to make observations as quickly as possible because the leakup introduced impurities and noise into the system. For this reason the observation time was limited to 1 ms and the Nyquist frequency arbitrarily set at 5 MHz for the pulse valve data.

This procedure was implemented at 25.0 eV (26.1 eV mean) first with xenon, which has a known ionization cross-section. Then it was repeated at the same energy for TEOS. The goal was to choose one TEOS ion peak and determine its cross-section by a cross reference with the xenon data as explained in Section 2.2. With one known data point the rest of the cross-sections were mapped out by the proportional relation between peak heights and cross-sections.

3.2.2 Cross-Section Measurements Measuring the partial ionization cross-sections was accomplished by taking TEOS spectra over and over at different energies and measuring the peak height of each ion at each energy. Since at this point mass resolution was not an issue, the observation time was changed to 10 ms and the Nyquist frequency was changed back to 2 MHz. This meant acquiring 40,000 data points instead of 200,000 which eased the computational burdens considerably. The electron beam energy range was set from 10 eV to 50 eV (11.1 eV to 51.1 eV mean)

in steps of 1 V. The lower limit was dictated by the uncertainty in the beam energy, which was ±1 Volt, and the upper limit was chosen so that electrons impacting on the Faraday cup were not energetic enough to produce secondary emission.

3.2.3 Ion Kinetics Measurements The ion kinetics work was accomplished by varying the time delay between ion creation and excitation. This allowed time for chemistry to occur. As the delay is varied in length one expects to see an evolution of the species as they are recorded at various stages of chemical interaction. The electron energy was held constant at 15.0 eV (16.1 eV mean) and the time delay varied between 10 ms and 470 ms in increments of 20 ms. This 20 ms increment then limited the observation time to 20 ms. It was decided that a 1 MHz Nyquist frequency was acceptable for this part of the experiment which meant 40,000 data points were acquired. Although this Nyquist frequency bounded the lowest observable mass at 30.4 a.m.u. , all the interesting chemistry proved to occur at much higher masses.

IV. Data/Discussion

Interpretation of the data required calibration of the frequency to mass conversion, pressure determination, and variation of the ion signal with electron energy.

4.1 Mass Calibration Data

The mass calibration was an iterative process designed to yield mass data with as few assumptions as possible. One problem with the frequency data was it tended to vary from experiment to experiment. That is, ion A^+ would be seen oscillating at some frequency during one experiment and at a slightly different frequency during another experiment. This was attributed to the buildup of space charge and its influence on the cyclotron frequency. Although the attempt was made to operate away from the space charge limit at all times, the frequency precision of the experiment was so good the effect of space charge was always seen. The solution to this problem was to devise a self-calibration strategy. That is, the ions contributing to the major mass peaks of the TEOS spectrum were determined and then the spectrum was calibrated assuming those peaks were known exactly. In this manner each TEOS spectrum was self-calibrated according to several of its own peaks.

4.1.1 Mass Calibration with Xenon and Air The first step in the calibration process was to pick several major TEOS peaks and determine which ions created them. This was done by cross referencing the TEOS spectrum with a xenon spectrum. TEOS mixed with xenon and air was introduced into the system giving the mass spectrum shown in Figure 4.1. For the record, the electron gun was run at 24.8±1 eV, 1000 transients were sum-averaged and the average electron beam throughput was on the order of one half nC.

The first mass scale applied to the spectrum was provided by Eq (2.1), which required knowing B. The magnetic field in the trap was previously measured by

Riehl and this value was applied. The idea was to identify the peaks due to oxygen, nitrogen, water vapor, and the three most abundant xenon isotopes and assume those masses to be precisely known according to current tables of atomic mass [12]. These peaks are characterized in Table 4.1.

Ion	Frequency (Hz)	Measured Mass (a.m.u.)	Known Mass (a.m.u.)
$^{132}Xe^+$	230550±40	131.98±0.02	131.90
$^{131}Xe^+$	232310±40	130.98±0.02	130.90
$^{129}Xe^+$	235920±40	128.98±0.02	128.90
O_2^+	951290±70	31.986±0.002	31.989
N_2^+	1086630±80	28.002±0.002	28.006
H_2O^+	1689800±100	18.007±0.001	18.010

Table 4.1. Xenon and Air Peaks According to Eq (2.1). These numbers characterize six of the peaks observed in Figure 4.1.

For the quadratic calibration, then, Eq (2.6) was applied to those six peaks giving $a_0 = 9.264\times10^{14}$, $b_0 = -1.143\times10^{10}$, and $c_0 = -6.400\times10^{6}$. The quadratic fit is illustrated in Figure 4.2. These calibration coefficients were then applied to the mass scale. This time seven distinct and evenly space TEOS peaks were identified along with the original six calibration peaks. They are listed in Table 4.2. The calibration was then worked for a second time using these seven peaks giving $a_0 = 9.264\times10^{14}$, $b_0 = -1.077\times10^{10}$, and $c_0 = -1.037\times10^{7}$. This quadratic fit is shown in Figure 4.3. Finally, these coeffients are applied to the mass scale with the results given in Table 4.3.

Table 4.3, which represents the best and final calibration, could have been expanded to characterize all the peaks in the TEOS spectrum, but this was not done for two reasons. First, the errors were large compared to Ledford *et. al.* [11] who used the same quadratic calibration approach to report a mass accuracy of 3 ppm on average. This suggested the experiment was operating within the space charge limit. Also, there was a concern about possible TEOS peaks buried beneath the strong

Ion	Frequency (Hz)	Measured Mass (a.m.u.)	Known Mass (a.m.u.)	Error (a.m.u.)	Error (ppm)
$SiO_4C_7H_{17}^+$	157420 ±30	193.09±0.04	193.0891	0.001	6
$SiO_4C_6H_{15}^+$	169760 ±40	179.07±0.04	179.0734	-0.0006	3
$SiO_3C_6H_{15}^+$	186430 ±30	163.08±0.03	163.0785	-0.002	10
$SiO_3C_5H_{13}^+$	203990 ±30	149.06±0.03	149.0628	0.004	24
$^{*132}Xe^+$	230550 ±40	131.90±0.02	131.9036	0.0001	1
$^{*131}Xe^+$	232310 ±40	130.90±0.02	130.9045	0.0006	5
$^{*129}Xe^+$	235920 ±40	128.91±0.02	128.9042	-0.0008	6
$SiO_2C_4H_{11}^+$	255460 ±40	119.05±0.02	119.0523	0.0005	4
$SiO_3H_3^+$	385170 ±50	78.98±0.01	78.9846	0.003	39
$^*O_2^+$	951290 ±70	31.989±0.002	31.98928	0.00001	<1
COH_3^+	981090 ±60	31.018±0.002	31.01784	0.00003	1
$^*N_2^+$	1086630±80	28.006±0.002	28.00560	0.00003	1
$^*H_2O^+$	1689800±100	18.010±0.001	18.01002	0.00002	1

Table 4.2. TEOS Peaks According to the Xenon and Air Calibration. Recalculating the mass axis according to the first set of coefficients gives the above mass assignments. The asterisk indicates the peaks which were used in the calibration.

Ion	Frequency (Hz)	Measured Mass (a.m.u.)	Known Mass (a.m.u.)	Error (a.m.u.)	Error (ppm)
$SiO_4C_7H_{17}^+$	157420±30	193.09±0.04	193.0891	0.002	11
$SiO_4C_6H_{15}^+$	169760±40	179.07±0.04	179.0734	-0.0008	4
$SiO_3C_6H_{15}^+$	186430±30	163.08±0.03	163.0785	-0.003	17
$SiO_3C_5H_{13}^+$	203990±30	149.06±0.03	149.0628	0.002	13
$SiO_2C_4H_{11}^+$	255460±40	119.05±0.02	119.0523	-0.002	14
$SiO_3H_3^+$	385170±50	78.98 ±0.01	78.9846	0.002	19
COH_3^+	981090±60	31.018±0.002	31.01784	-0.0002	7

Table 4.3. TEOS Peaks According to the Self-Calibration. Recalculating the mass axis again according the second set of coefficients gives the above mass assignments.

xenon peaks. Since seven major TEOS peaks were resolvable without ambiguity in spite of the marginal mass accuracy, it seemed better to start again and apply the self-calibration approach to a pure TEOS spectrum ionized with a smaller shot of electrons.

4.1.2 The TEOS Mass Spectrum Once the self-calibration approach was devised, it was applied to a spectrum of pure TEOS for the purpose of thoroughly characterizing it. Again, for the record this spectrum was taken under the following conditions: 25.0 eV electron energy (26.1 eV mean), 0.075±0.002 nC charge throughput, and 1000 transient sum averages. Notice the electron gun was tuned down consirably with the hope of avoiding the space charge limit. Figures 4.4 through 4.7 display this spectrum in detail. The peaks identified in this spectrum are characterized on Tables 4.4 and 4.5.

As one can see, the TEOS mass spectrum is quite rich with ions. Some of the ion peaks were determined to be the result of heavier atomic isotopes in the TEOS constituants as opposed to an additional hydrogen atom. For example, the ion at 194 a.m.u. could have been $SiO_4C_7H_{18}^+$, one hydrogen atom above the strong $SiO_4C_7H_{17}^+$ peak. A closer examination of the masses, however, suggested that a combination of $^{29}SiO_4C_7H_{17}^+$ and $SiO_4^{13}CC_6H_{17}^+$ was responsible for the peak. While $Si^{17}OO_3C_7H_{17}^+$ and $SiO_4C_7^2HH_{16}^+$ doubtlessly contributed to the peak as well, their natural abundances are so low, even when taken in combinations of 4 and 17, that their contributions were beneath the sensitivity of the instrument. This pattern of ion at mass m with isotopic contributions at masses $m+1$ and $m+2$ was repeated for $SiO_4C_8H_{20}^+$ (the parent TEOS ion), $SiO_4C_6H_{15}^+$, $SiO_3C_6H_{15}^+$, $SiO_3C_5H_{13}^+$, $SiO_3C_4H_{11}^+$, and $SiO_2C_4H_{11}^+$.

Ion	Frequency (Hz)	Measured Mass (a.m.u.)	Known Mass (a.m.u.)	Error (a.m.u.)	Error (ppm)
$SiO_4^{13}CC_7H_{20}^+$ $^{29}SiO_4C_8H_{20}^+$	145360±30	209.12±0.04	209.1159	-0.0004	2
$SiO_4C_8H_{20}^+$	146060±30	208.11±0.04	208.1125	-0.0003	1
$SiO_4C_8H_{19}^+$	146770±20	207.11±0.03	207.1047	-0.0016	8
$^{30}SiO_4C_7H_{17}^+$	155830±20	195.10±0.02	195.0859	-0.0010	5
$^{29}SiO_4C_7H_{17}^+$ $SiO_4^{13}CC_6H_{17}^+$	156630±20	194.10±0.03	194.0886	-0.0007	4
$SiO_4C_7H_{17}^+$	157440±20	193.09±0.03	193.0891	0.0005	3
$^{30}SiO_4C_6H_{15}^+$	167900±30	181.07±0.03	181.0703	-0.0042	23
$^{29}SiO_4C_6H_{15}^+$ $SiO_4^{13}CC_5H_{15}^+$	168830±20	180.07±0.02	180.0730	-0.0011	6
$SiO_4C_6H_{15}^+$	169780±20	179.07±0.02	179.0734	0	<1
$SiO_4C_5H_{13}^+$	184210±30	165.06±0.02	165.0578	-0.0001	1
$SiO_3^{13}CC_5H_{15}^+$ $^{29}SiO_3C_6H_{15}^+$	185310±30	164.08±0.02	164.0818	0.0009	5
$SiO_3C_6H_{15}^+$	186450±20	163.08±0.02	163.078	-0.0005	3
$SiO_4C_4H_{11}^+$	201330±20	151.04±0.01	151.0421	0.0001	1
$^{29}SiO_3C_5H_{13}^+$ $SiO_3^{13}CC_4H_{13}^+$	202640±20	150.06±0.02	150.0624	-0.0016	11
$SiO_3C_5H_{13}^+$	204000±20	149.06±0.01	149.0628	0	<1
$SiO_4C_3H_9^+$	221940±20	137.03±0.01	137.0265	-0.0002	1
$SiO_3^{13}CC_3H_{11}^+$ $^{29}SiO_3C_4H_{11}^+$	223530±30	136.05±0.01	136.0505	0.0009	7

Table 4.4. The TEOS Mass Spectrum. Applying the self-calibration procedure described in the previous section gives the above mass assignments.

Ion	Frequency (Hz)	Measured Mass (a.m.u.)	Known Mass (a.m.u.)	Error (a.m.u.)	Error (ppm)
$SiO_3C_4H_{11}^+$	225190±20	135.05±0.01	135.0472	-0.0003	2
$SiO_4C_2H_7^+$	247250±20	123.01±0.01	123.01081	-0.00015	1
$SiO_3C_3H_9^+$	251290±20	121.03±0.01	121.03155	-0.00004	0.3
$SiO_2^{13}CC_3H_{11}^+$ $^{29}SiO_2C_4H_{11}^+$	253340±20	120.05±0.01	120.0556	0.0017	14
$SiO_2C_4H_{11}^+$	255470±20	119.05±0.01	119.05228	-0.00009	1
$SiO_4CH_7^+$	274000±20	111.01±0.01	111.01081	0.00060	5
$SiO_3C_2H_7^+$	284230±20	107.02±0.01	107.01590	0.00012	1
$SiO_2C_3H_9^+$	289590±20	105.04±0.01	105.03663	-0.00047	4
$SiO_2C_3H_7^+$	295260±20	103.02±0.01	103.02098	0.00031	3
$SiO_3CH_5^+$	327100±20	93.001±0.004	93.00025	-0.00022	2
$SiO_2C_2H_7^+$	334210±20	91.021±0.005	91.02098	0.00005	1
$SiO_3H_3^+$	385170±20	78.984±0.004	78.98460	0.00026	3
$SiO_2CH_5^+$	395080±20	77.0052±0.004	77.00533	0.00013	2
$SiO_2H_3^+$	483030±20	62.990±0.003	62.9897	0.00024	4
$OC_2H_6^+$	660910±50	46.041±0.003	46.04132	0.00048	10
$OC_2H_5^+$	675700±20	45.033±0.002	45.03349	0.00040	9
$SiOH^+$	676520±20	44.979±0.002	44.97912	0.00022	5
OCH_3^+	981100±50	31.018±0.002	31.01784	-0.00004	1

Table 4.5. The TEOS Mass Spectrum (Continued). Applying the self-calibration procedure described in the previous section gives the above mass assignments.

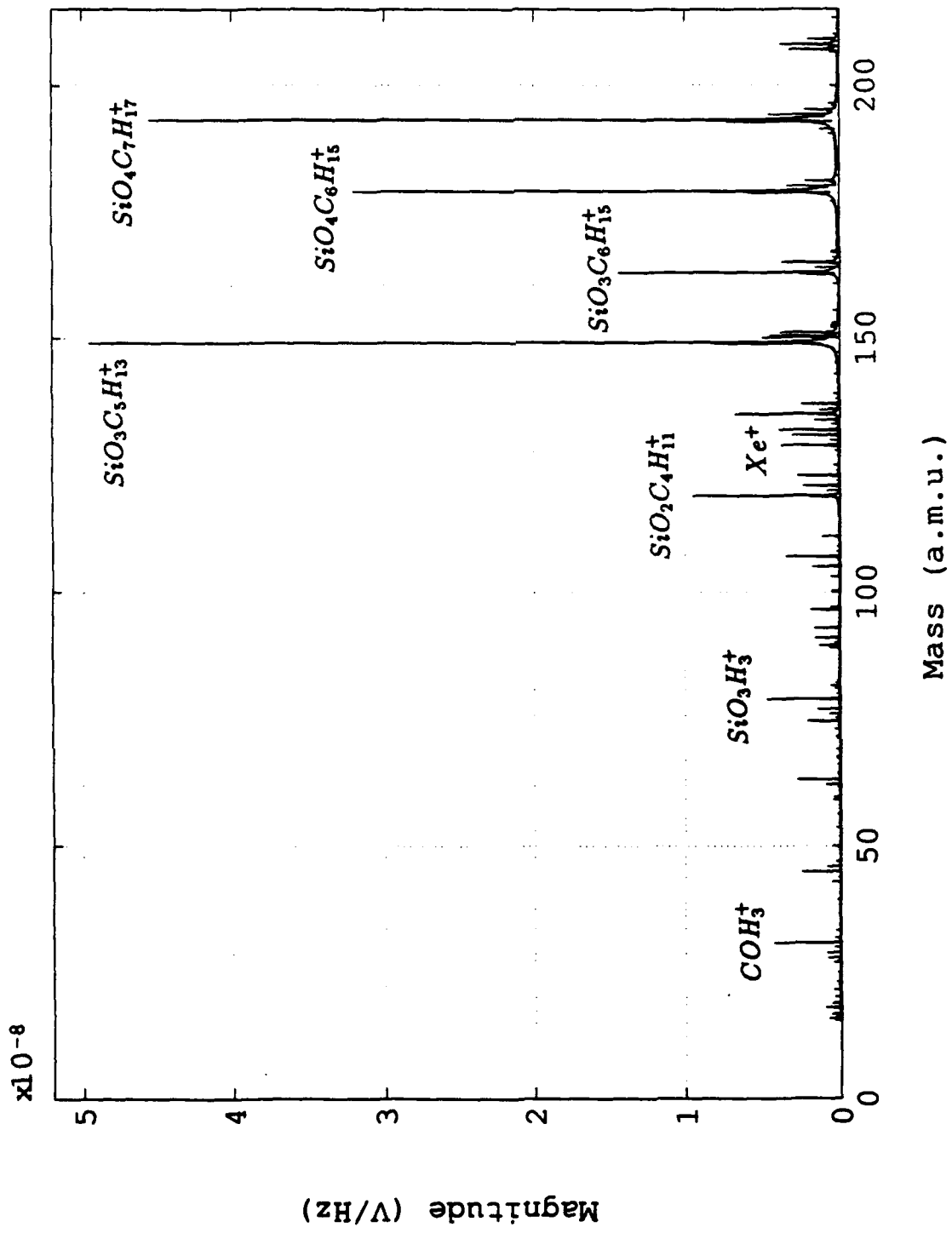

Figure 4.1. TEOS Calibration Spectrum with Xenon and Air. This spectrum was acquired with a 50 ms observation time at a 2 MHz Nyquist frequency.

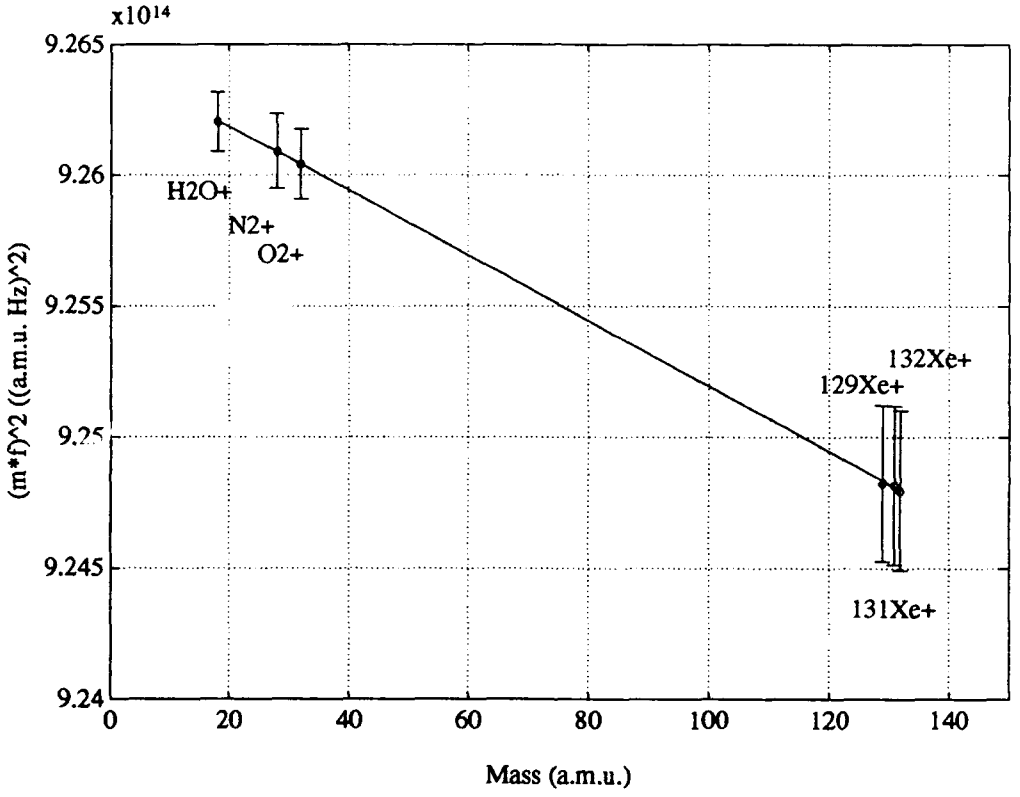

Figure 4.2. Mass Calibration with Xenon and Air. This is the quadratic calibration applied to six calibration peaks provided by xenon and air. The error bars are derived from the frequency uncertainty.

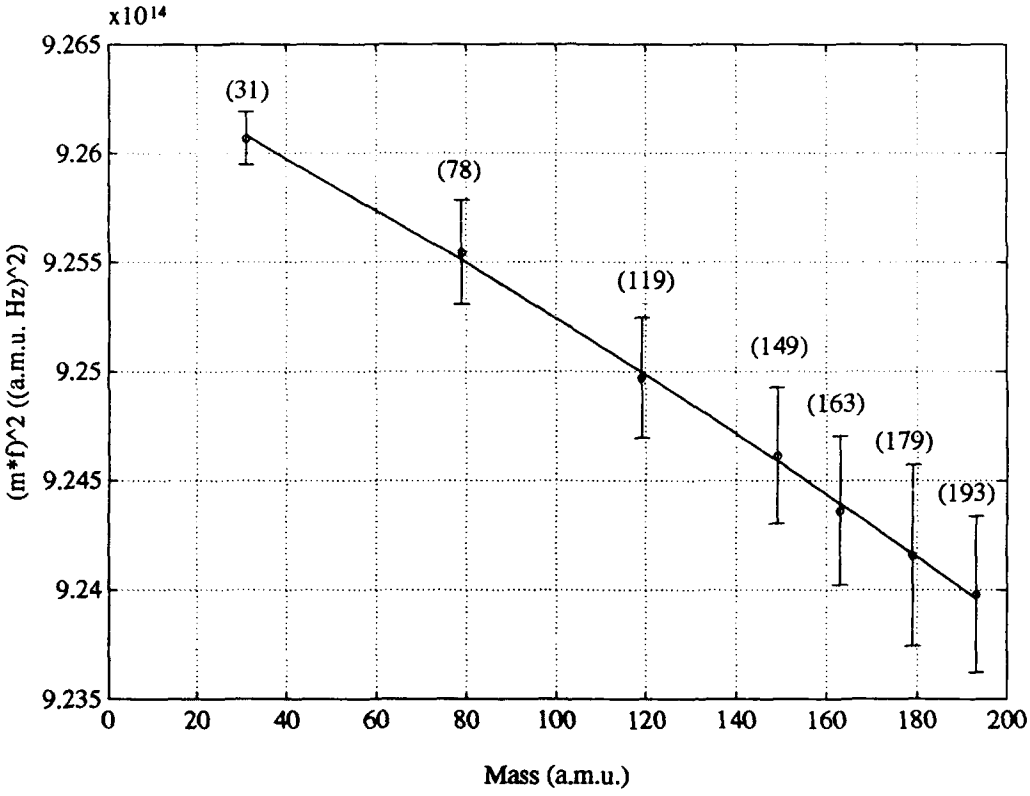

Figure 4.3. Mass Calibration with Major TEOS Peaks. This is the quadratic calibration applied to the seven evenly spaced TEOS peaks. The number in parentheses is the mass of each peak rounded down. See Tables 4.4 and 4.5 to match the ion to the mass. Again the error is a result of the frequency uncertainty.

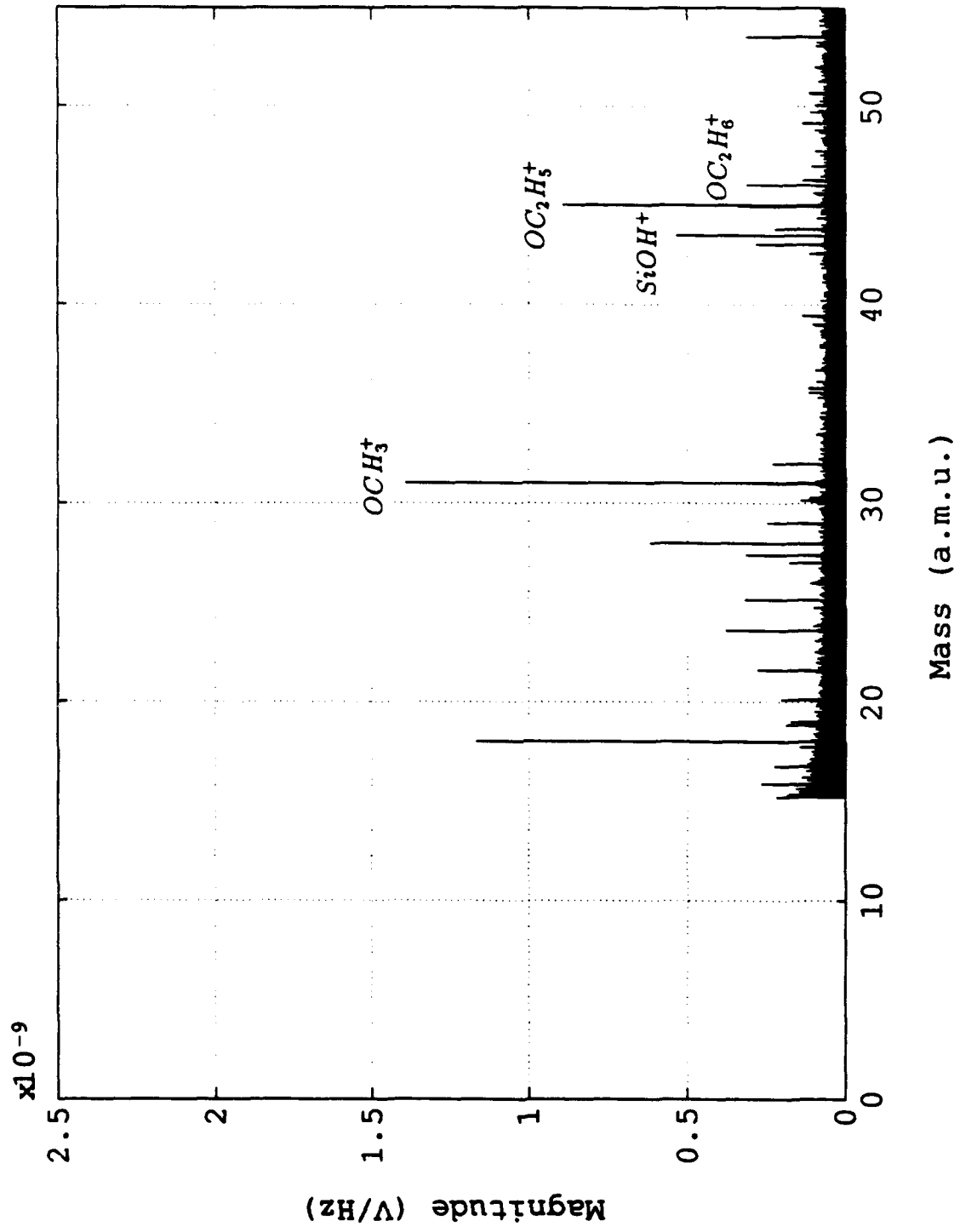

Figure 4.4. TEOS Self-Calibration Spectrum from 0 to 55 a.m.u. This spectrum was acquired with a 50 ms observation time at a 2 MHz Nyquist frequency.

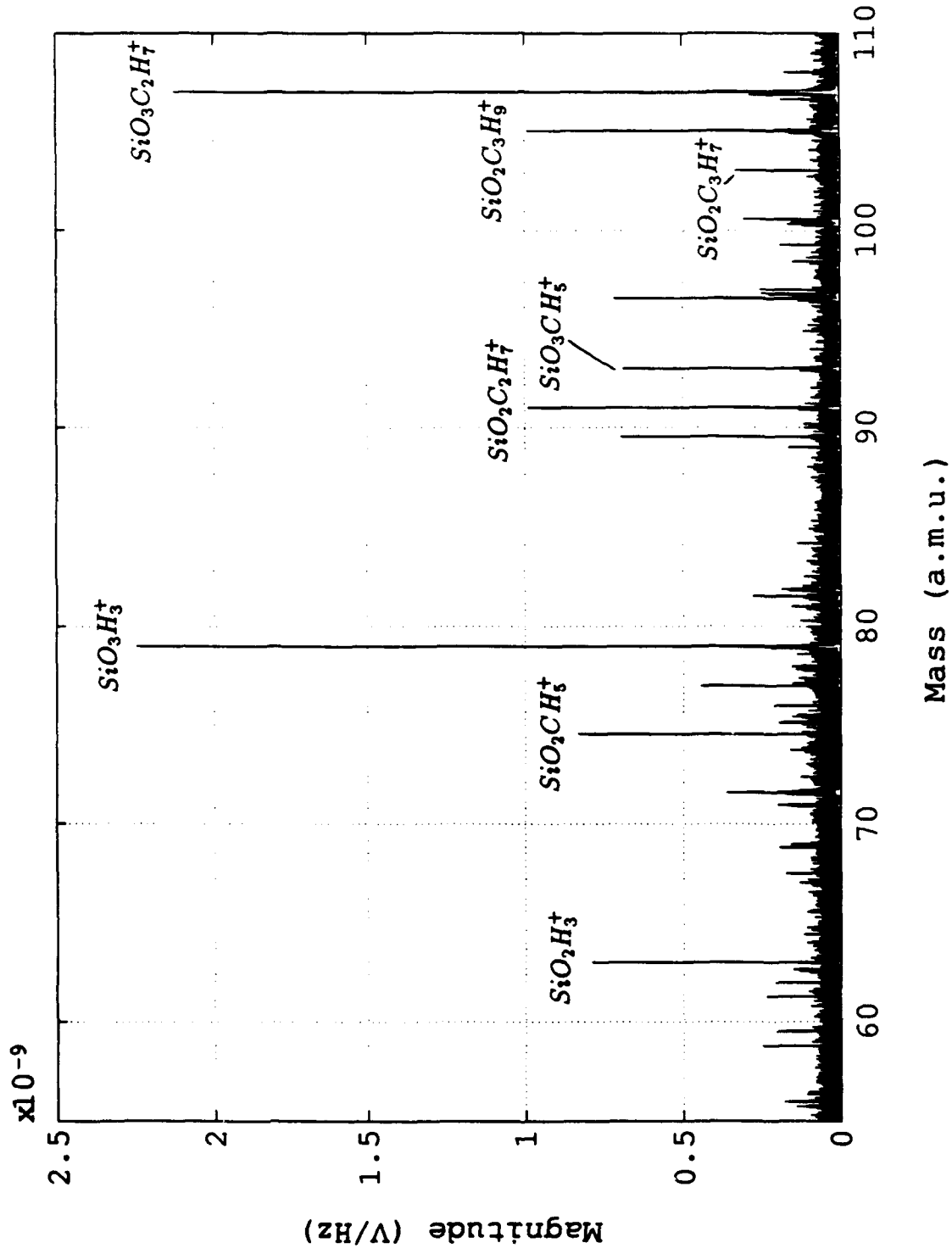

Figure 4.5. TEOS Self-Calibration Spectrum from 55 to 110 a.m.u. This spectrum was acquired with a 50 ms observation time at a 2 MHz Nyquist frequency.

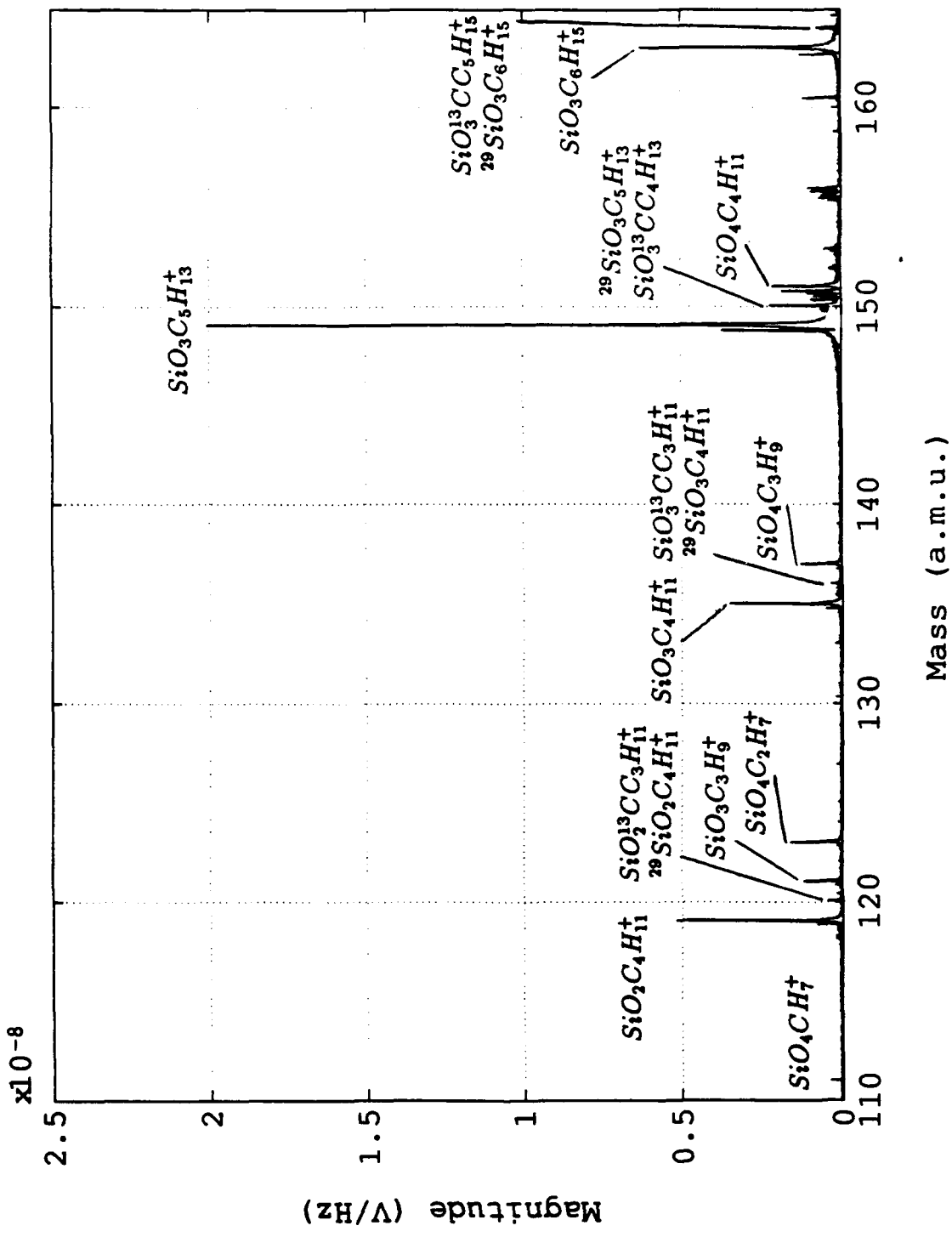

Figure 4.6. TEOS Self-Calibration Spectrum from 110 to 165 a.m.u. This spectrum was acquired with a 50 ms observation time at a 2 MHz Nyquist frequency.

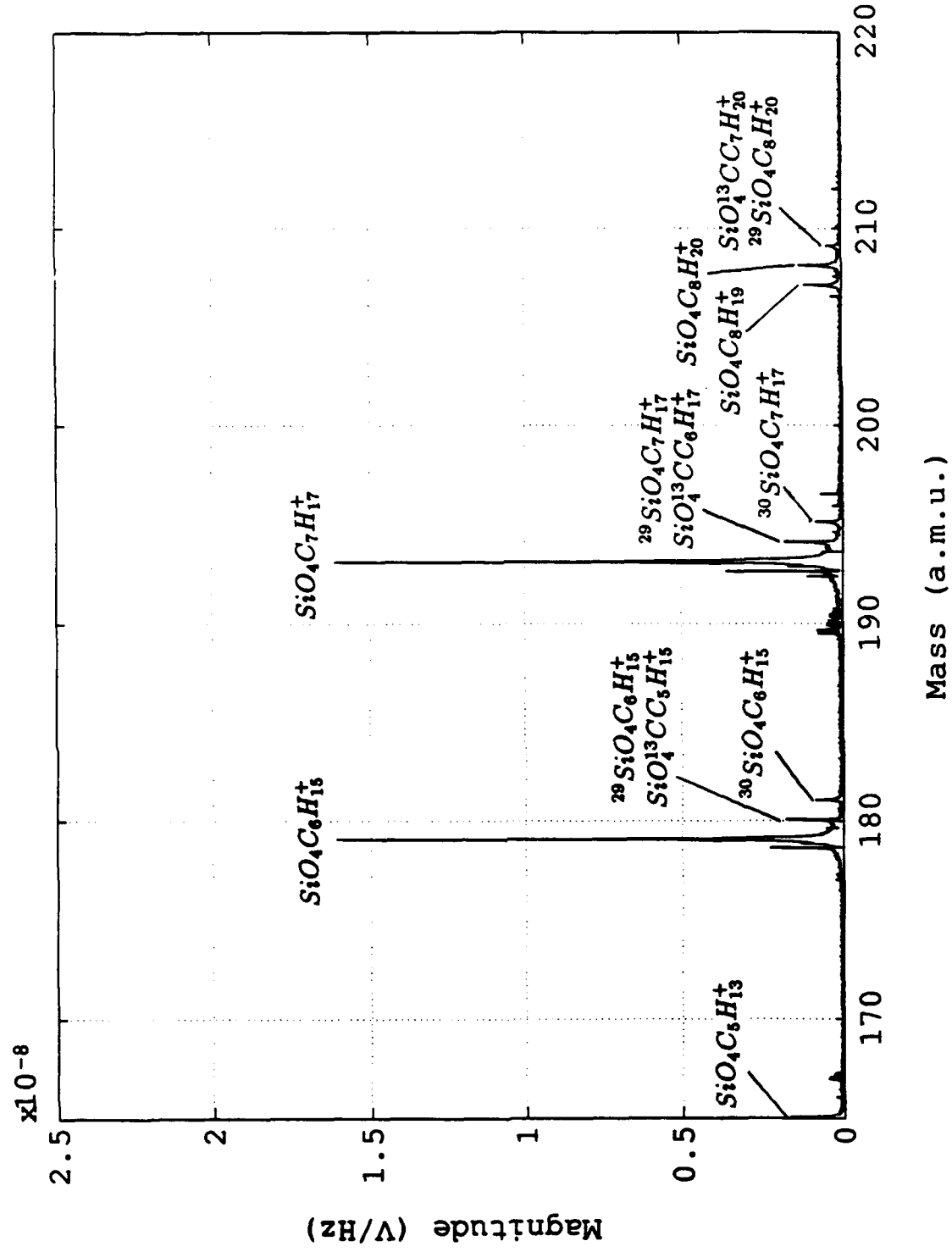

Figure 4.7. TEOS Self-Calibration Spectrum from 165 to 220 a.m.u. This spectrum was acquired with a 50 ms observation time at a 2 MHz Nyquist frequency.

4.2 Pulse Valve Pressure Calibration

Once the mass spectrum was calibrated along the mass axis the pulse valve pressure measurements were performed to establish the calibration along the intensity axis.

4.2.1 Xenon First the pressure per puff was measured for xenon as shown in Figure 4.8. These results are represented with the leakup rate subtracted off. The anomolous bump at 55 seconds was the result of vibrations caused by closing the gate valve. Each jump in pressure corresponded to 16 puffs of xenon. Working out the numbers the pressure per puff was found to be $(2.23\pm0.04)\times10^{-7}$ Torr/puff.

Next, the xenon spectrum was taken at known pressures by closing the gate valve and puffing in gas as shown in Figure 4.9. A plot of total peak intensity versus pressure, presented in Figure 4.10, gives a line whose slope relates peak intensity to number ions in the trap since pressure and the number of ions are analogous.

Note the magnitude appears to flatten at pressures above 1.5×10^{-6} Torr. This was attributed to the presence of space charge in the trap. At such high pressures so many ions were created that their collective self-field pushed many of them out of the trap thus reducing the signal. With this in mind, the line was only fit to the first five data points giving a slope of 2.50 ± 0.07 V/Hz/C/Torr.

4.2.2 TEOS The pressure per puff experiment was repeated for TEOS as shown in Figure 4.11. Each jump in pressure corresponded to 250 puffs of gas. This number had to be so large compared to the xenon experiment because the vapor pressure of TEOS in the manifold was so low. Each step appeared to have a distinct pressure profile which contributed to the uncertainty in the pressure. Also, this plot was chopped off at 8×10^{-6} Torr because the pressure readings from the spinning rotor gauge above this value depended on knowing the viscosity of TEOS, which was not known. The pressure per puff was found to be $(7.4\pm0.6)\times10^{-9}$ Torr/puff.

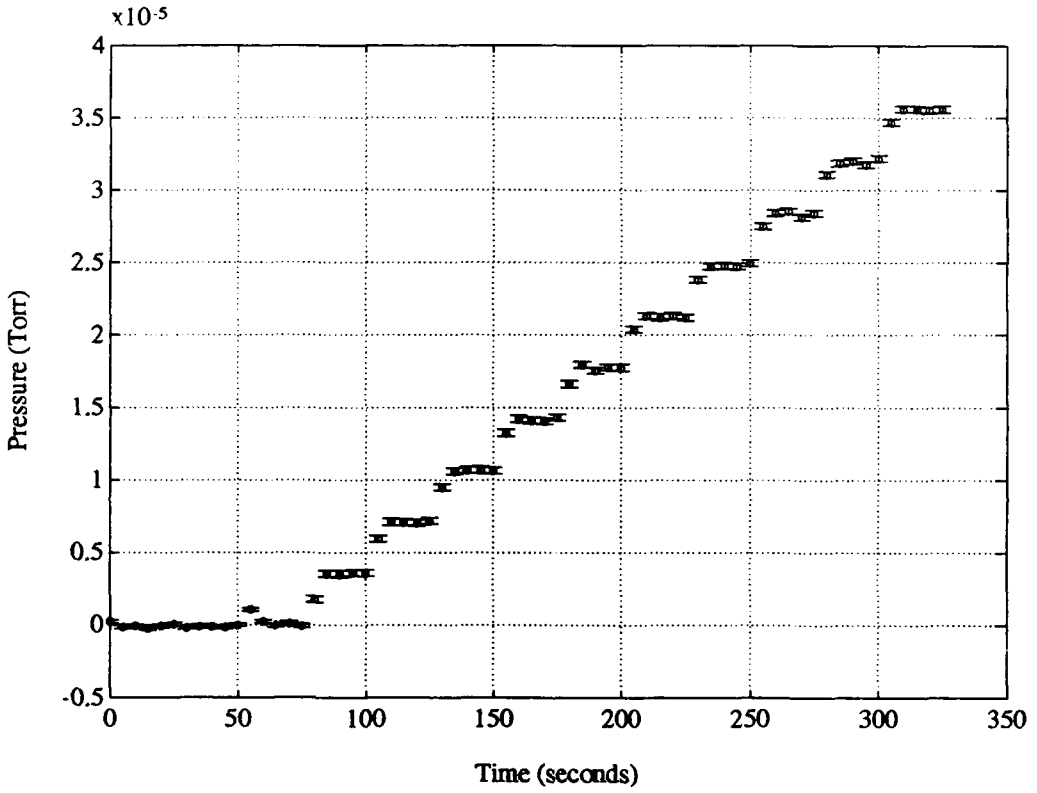

Figure 4.8. Xenon Pulse Valve Pressure Calibration Results. This plot shows the readings on the spinning rotor gauge as a function of time as xenon is puffed into the system. The background leakup rate has been subtracted.

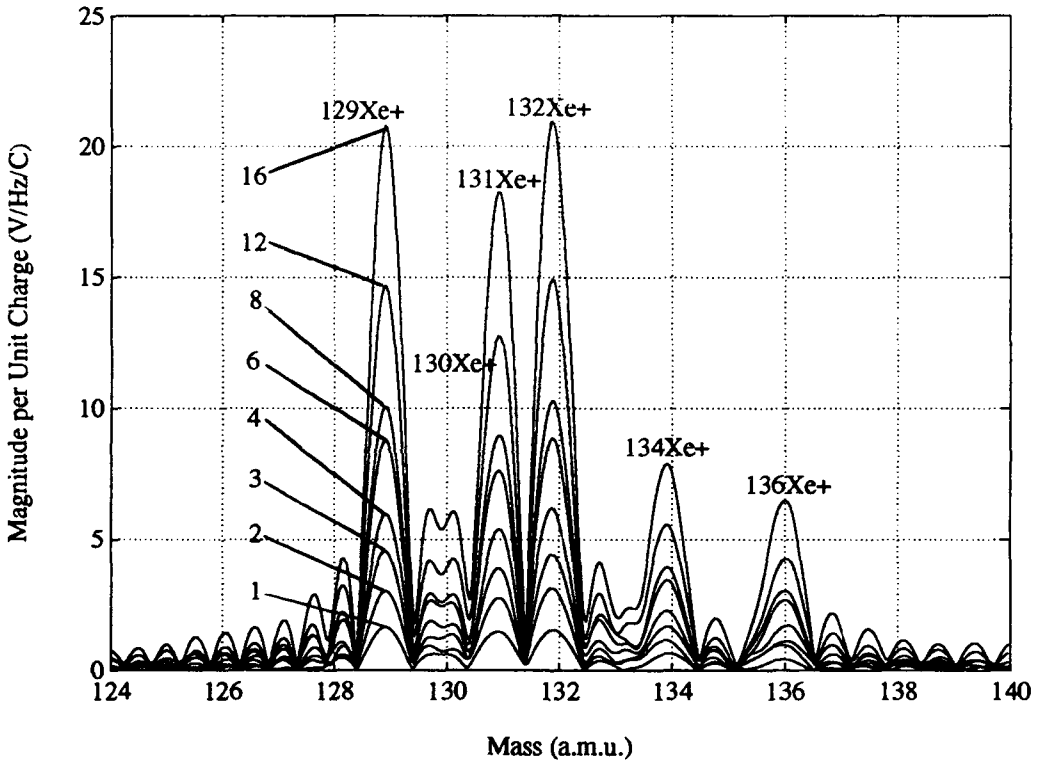

Figure 4.9. Xenon Peaks at Known Pressures. At this resolution xenon has six isotopes. Indicated are the number of puffs required to produce each signal.

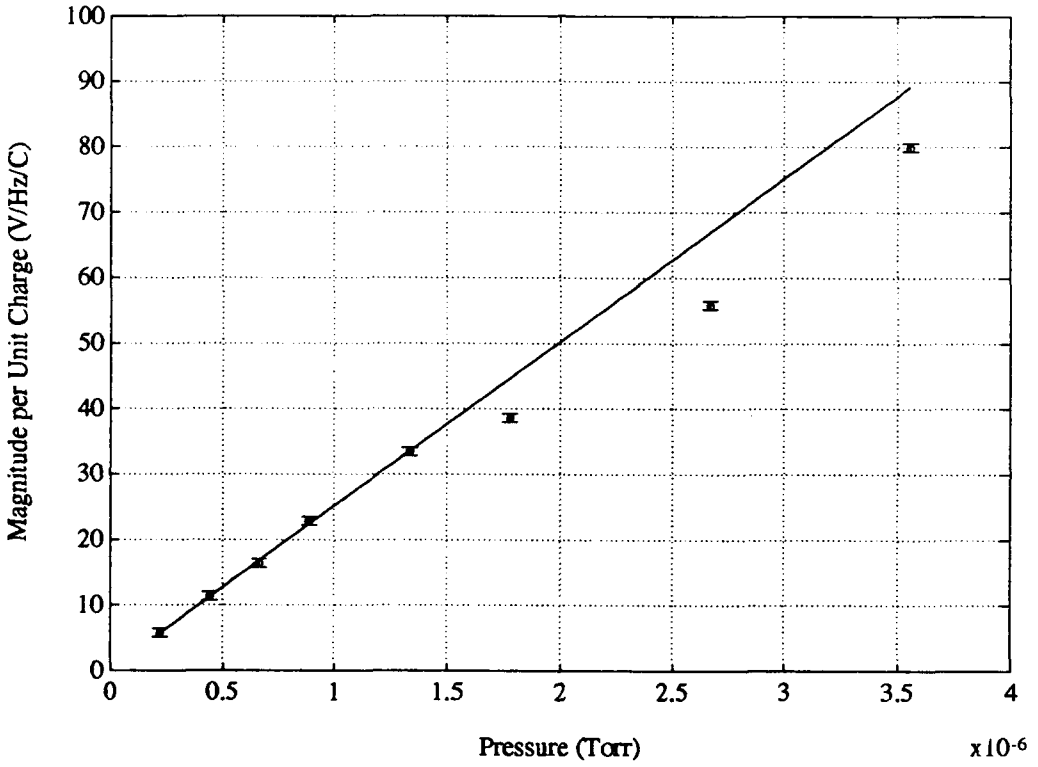

Figure 4.10. Xenon Peak Magnitude to Pressure Correlation. Plotting signal intensity as a function of pressure shows the linear relation. All the isotopes are summed to generate the total intensity. The error bars are derived from the uncertainties in the peak intensity and beam current.

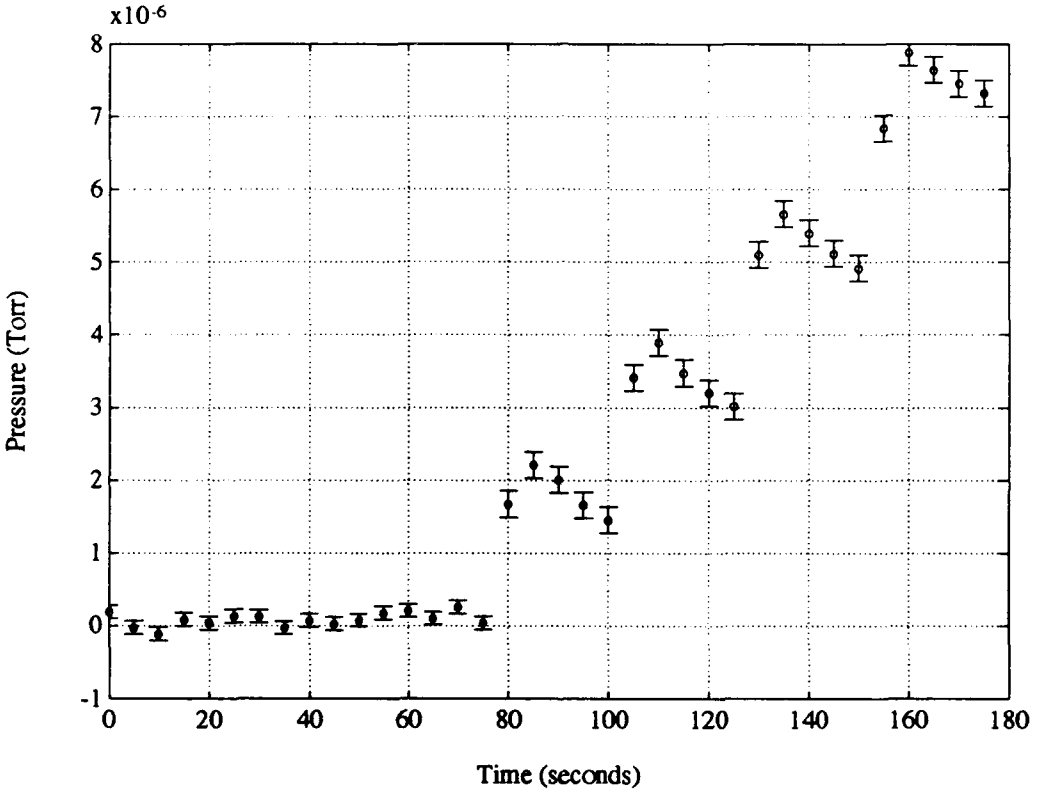

Figure 4.11. TEOS Pulse Valve Pressure Calibration Results. This plot shows the readings on the spinning rotor gauge as a function of time as TEOS is puffed into the system.

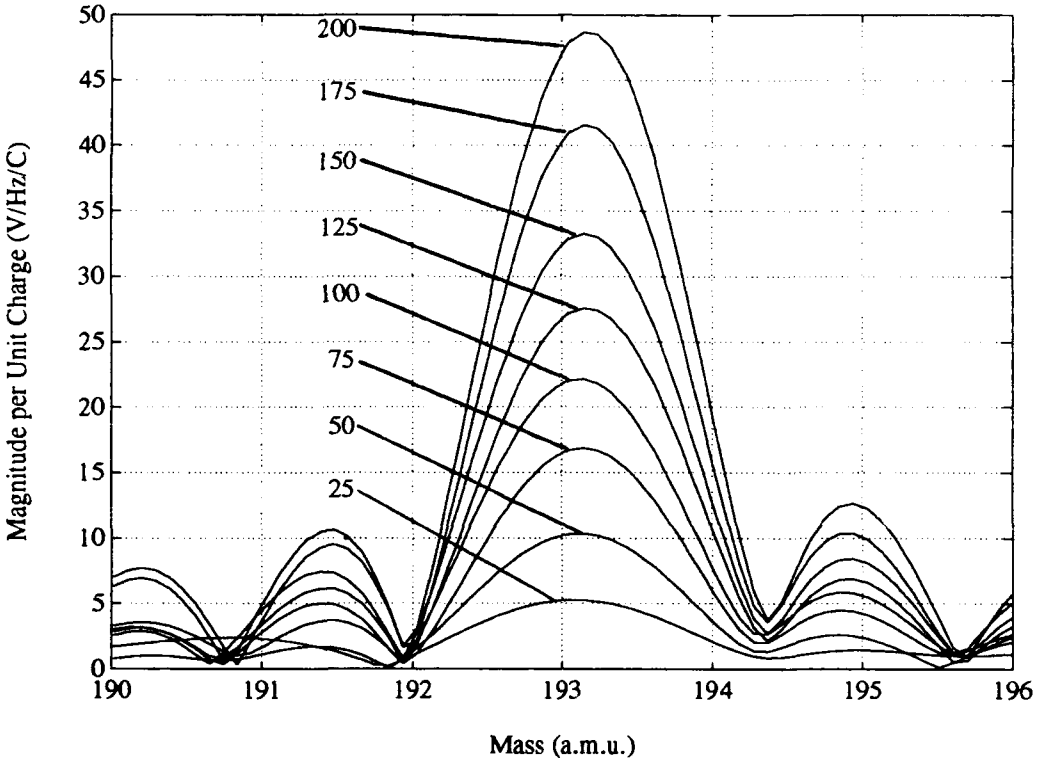

Figure 4.12. $SiO_4C_7H_{17}^+$ Peaks at Known Pressures. Indicated are the number of puffs required to produce each signal.

Next, the TEOS spectrum was taken after closing the gate valve and puffing in gas as shown in Figure 4.12. The $SiO_4C_7H_{17}^+$ peak at 193 a.m.u. was chosen as the one to be referenced as it seemed to be the clearest and most consistant.

Again the peak height was plotted as a function of pressure as presented in Figure 4.13 giving a slope of 3.3±0.1 V/Hz/C/Torr. With this data and knowing the cross-section of xenon at 26.1 eV ($(3.61\pm0.43)\times10^{-16}$ cm^2 [20]) the partial ionizaton cross-section of $SiO_4C_7H_{17}^+$ at 26.1 eV was found to be $(4.82\pm0.57)\times10^{-16}$ cm^2.

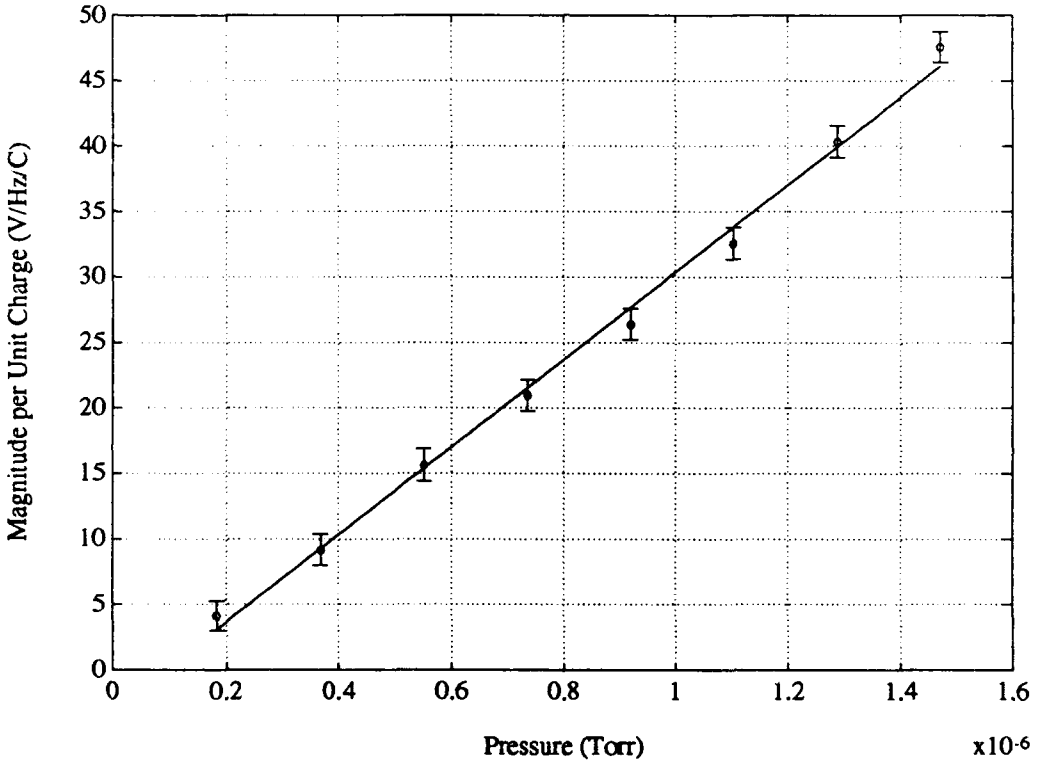

Figure 4.13. Plotting signal intensity as a function of pressure shows the linear relation. Again the error bars are a result of the uncertainties in the peak intensity and beam current.

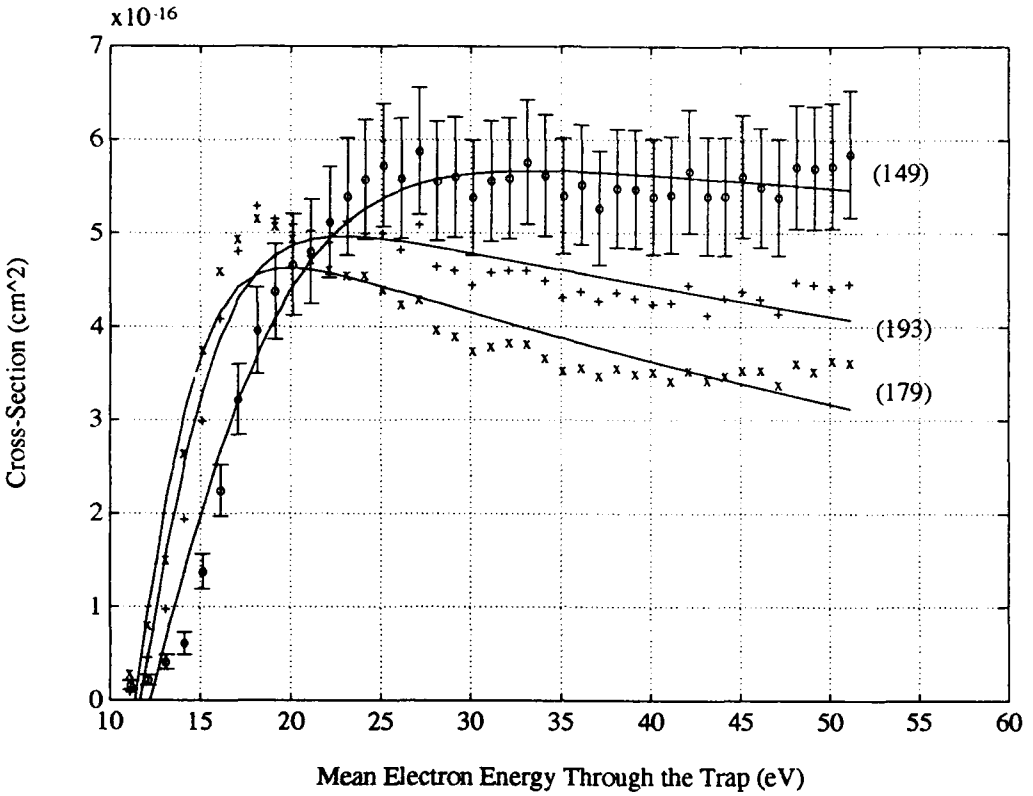

Figure 4.14. Some Typical Cross-Sections. These cross-section curves were found to be the dominant contributions to the total ionization cross-section. The parameterization of these curves, which will be discussed shortly, is plotted as well. The designator in parentheses is the mass of the ion rounded down. See Table 4.4 to match the ion to the mass.

4.3 The Cross-Sections

Once the partial ionization cross-section of $SiO_4C_7H_{17}^+$ was determined from the pulse valve experiment, it was applied to the cross-section data. Out of the 35 ions identified in Tables 4.4 and 4.5 cross-sections were measured for 24 of them. The remaining 11 had ion signals which were so weak their cross-sections were not discernable above noise. While data for the three most abundant ions are shown in Figure 4.14, the rest of the curves can be found in Appendix A.

The uncertainties in the cross-sections are based on the uncertainties in the pressure calibration and reference cross-section. The reference cross-section was known to about 12 percent and was the dominant factor in the uncertainties presented here. Another contribution to the error, which was not incorporated in this analysis, was the fluctuation of pressure in the trap. This was shown by small variations in the cross-section common to all three curves. This effect was dealt with experimentally by completing the data acquisition as quickly as possible and by taking data points in random order.

Displayed in Figure 4.15 are seven cross-sections which exhibited an unexpected resonance between 10 and 18 eV. This resonance appears to be associated with the breaking of an $Si - O$ bond and suggests a large number of excited states which decay through the breaking of this bond. While this feature only appeared in the lower mass ions, not all lower mass ions showed this resonance.

Summing up all the partial cross-section curves gives the total electron impact ionization cross-section for TEOS as shown in Figure 4.16. As expected from a molecule with 33 constituant atoms, it is quite large. Also, it levels off at a fairly low energy. This too is expected behavior from large molecules as they are like large atoms whose outer electrons are loosely bound and easily liberated. Note that the unusual resonances observed in some of the partial ionization cross-sections make small contributions to the total cross-section and are not observed.

The data for the 17 well-behaved cross-sections can be represented with the following functional parameterization:

$$\sigma(\epsilon - T) = Ae^{-k(\epsilon - T)} \tanh(\frac{\pi(\epsilon - T)}{\alpha}) \tag{4.1}$$

where σ is the cross-section, ϵ is the electron energy, T is the appearance potential, A scales the amplitude, k characterizes the higher energy behavior of σ, and α describes $\frac{d\sigma}{d\epsilon}$ near threshold. These parameters are given in Table 4.6.

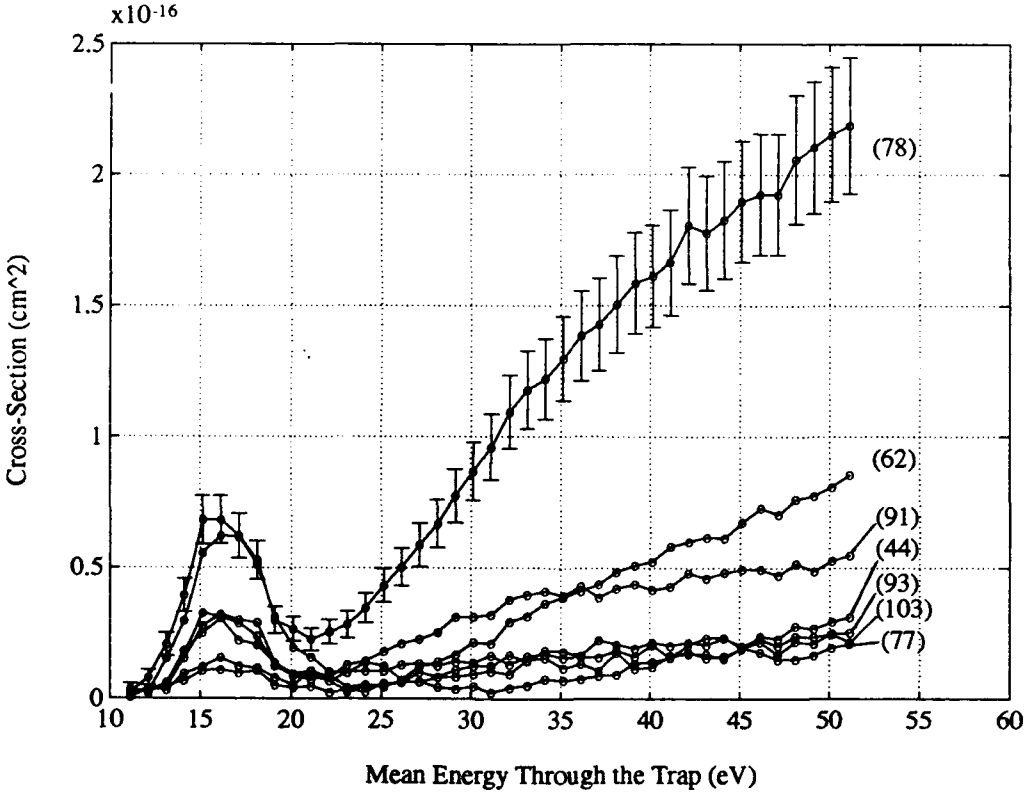

Figure 4.15. Cross-Sections with the Unexpected Resonance. 7 of the 24 ions showed this unusual resonance at low energies. Compared to Figure 4.14, however, their contributions to the total cross-section were small.

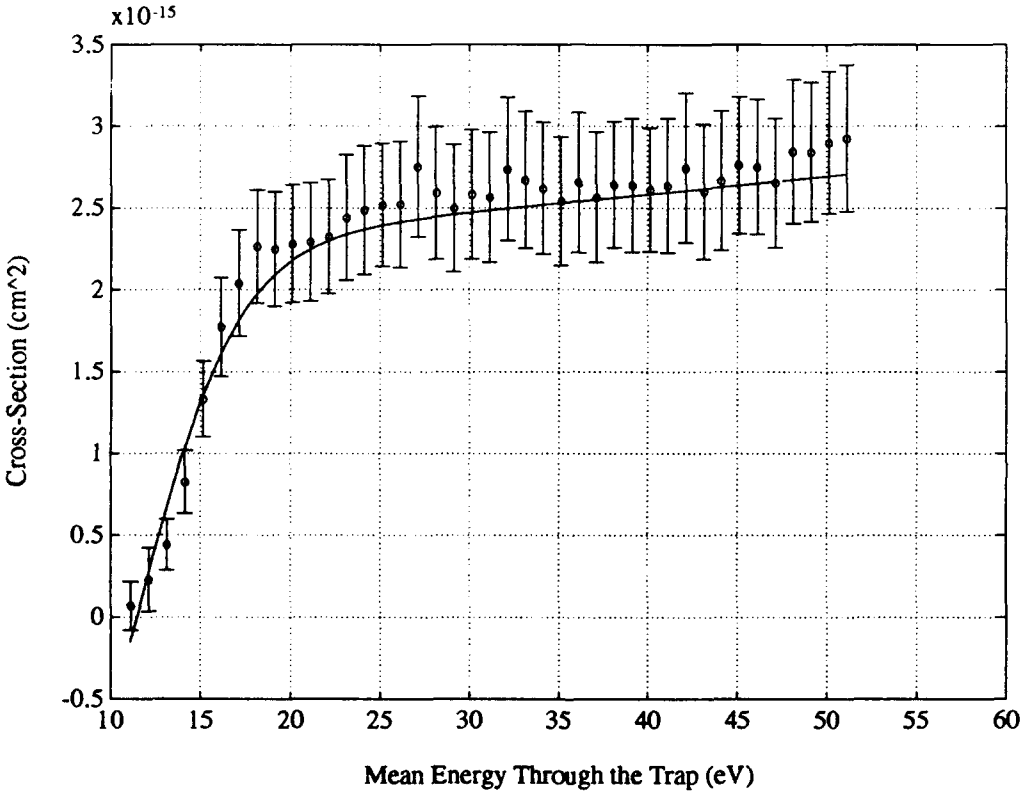

Figure 4.16. TEOS Total Ionization Cross-Section. Summing up the 24 partial ionization cross-sections gives the total ionization cross-section.

Ion	A×10^{16} (cm^2)	k×100 (eV^{-1})	α (eV)	T (eV)
$SiO_4C_8H_{20}^+$	0.5601	0.3485	13.7104	11.6468
$SiO_4C_8H_{19}^+$	0.3158	0.1298	17.6743	11.4340
$SiO_4C_7H_{17}^+$	5.5097	0.7649	14.9716	11.7007
$SiO_4C_6H_{15}^+$	5.3357	1.3482	12.4299	11.3903
$SiO_4C_5H_{13}^+$	0.4610	0.4642	23.0881	12.2065
$SiO_3C_6H_{15}^+$	2.0320	0.1326	35.6666	11.6557
$SiO_4C_4H_{11}^+$	0.6854	0.8440	17.6266	11.6844
$SiO_3C_5H_{13}^+$	6.0627	0.2652	25.7422	12.2107
$SiO_4C_3H_9^+$	0.3371	0.3074	27.2577	12.2137
$SiO_3C_4H_{11}^+$	1.0542	0.1451	32.7496	12.0646
$SiO_3C_3H_9^+$	0.3926	0.1688	43.6311	12.3019
$SiO_2C_4H_{11}^+$	2.1405	0.2760	57.1502	13.4282
$SiO_3C_2H_7^+$	0.8201	0.0821	64.7240	12.7807
$SiO_2C_3H_9^+$	0.3564	0.3172	68.1769	10.6960
$OC_2H_6^+$	0.1615	0.8448	12.4848	11.5110
$OC_2H_5^+$	0.4304	0.5828	11.4414	11.6284
OCH_3^+	0.8897	0.7775	16.5643	12.0059
total	22.9251	-0.4188	17.2907	11.4661

Table 4.6. Fitting Parameters. These parameter are used with Eq (4.1) to fit the data for the 17 of the 24 cross-sections.

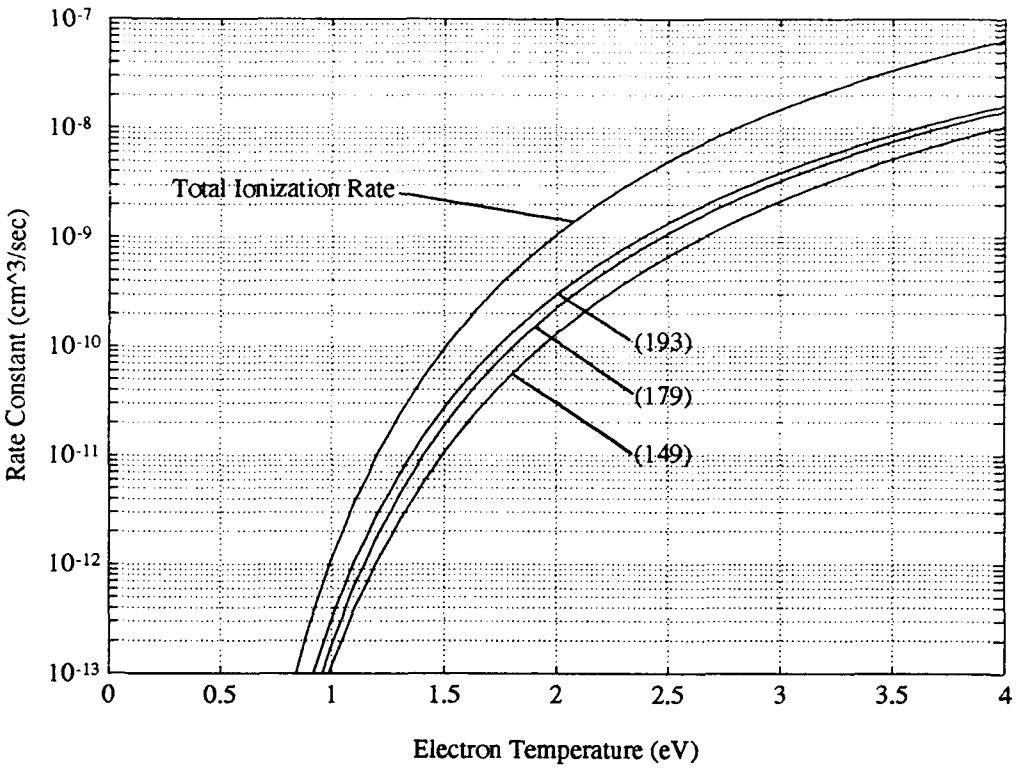

Figure 4.17. Ionization Rates. Assuming a Maxwellian energy distribution, the cross-section data allows one to calculate the ionization rates according to Eq (2.17). This plot shows the total ionization rate along with the partial ionization rates for the three most abundantly produced species.

With the cross-section data the production rates for the various species was calculated as described in Section 2.2. Figure 4.17 shows the results of this calculation for the total ion production rate as well as the rates for the three most abundantly produced species.

Ion	Measured Mass (a.m.u.)
$SiO_3C_5H_{13}^+$	149.06 ± 0.04
$SiO_3C_6H_{15}^+$	163.08 ± 0.04
$SiO_4C_6H_{15}^+$	179.07 ± 0.05
$SiO_4C_7H_{17}^+$	193.09 ± 0.07
$SiO_4C_8H_{19}^+$	207.11 ± 0.06
$SiO_4C_8H_{20}^+$	208.11 ± 0.09
$SiO_4C_8H_{21}^+$	209.12 ± 0.09
	283.1 ± 0.1
	297.2 ± 0.1
	315.2 ± 0.1
	343.2 ± 0.1
	357.2 ± 0.2
	371.3 ± 0.2
	417.3 ± 0.2
	431.3 ± 0.2

Table 4.7. Ion Chemistry Reactants and Products. These ions were identified as playing significant roles in the ion chemistry. Above 208 a.m.u. it was not possible to determine the chemical composition of the ions unambiguously.

4.4 Ion Chemistry

Although 35 different ions are formed when electrons impact on TEOS, most occure in such small concentrations that they were ignored for the chemical kinetics experiment. Table 4.7 lists the major ions participating in the ion chemistry. Six of these are created upon electron impact and were identified previously. The rest arise as a result of the ion chemistry. While their masses are known, it is no longer possible in this experiment to determine the species based on mass alone. This is because all the new ions occur at large masses where the uncertainties become large as well. If the uncertainties become too large than it is possible to find more than one plausible arrangement of atoms whose mass lies within that uncertainty.

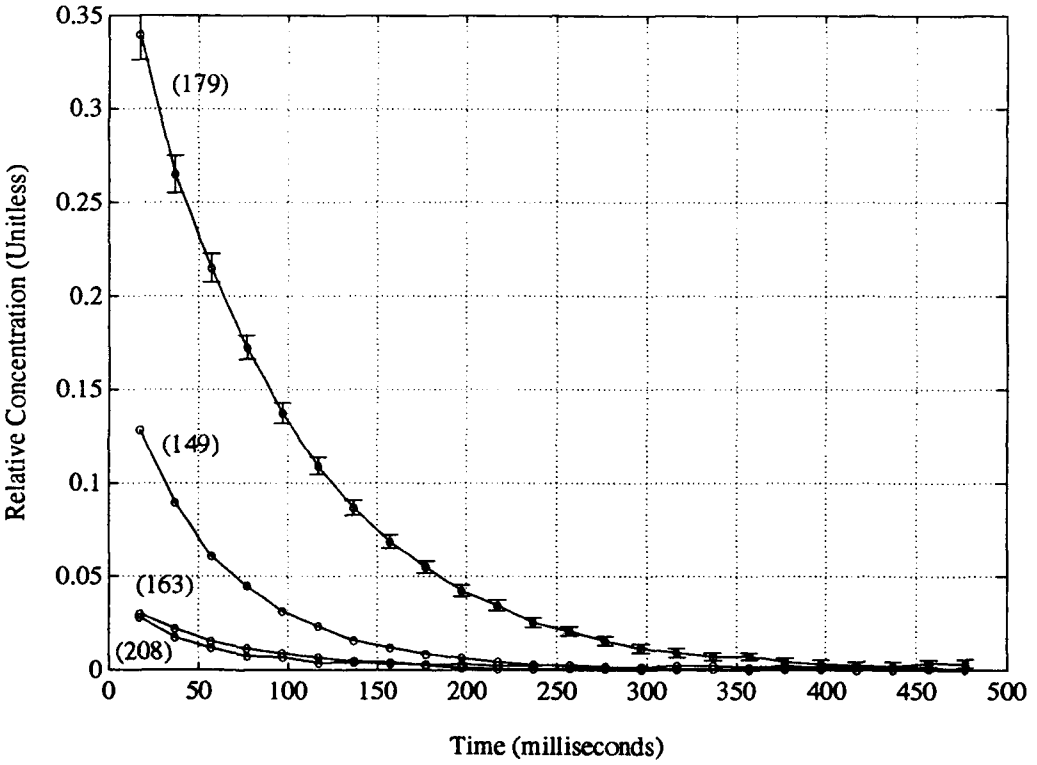

Figure 4.18. Decay Curves for Masses 208, 179, 163, and 149. These four ions produced by 15.0 eV electron impact were only consumed and decayed exponentially with time.

Four of the original six reactants decayed exponentially in time as shown in Figure 4.18. Time constants from these plots were determined and are presented in Table 4.8. With the pulse valve calibration data it was possible to determine the pressure at which the chemical kinetics experiment was performed. As with the cross-section data this was done by comparing the peak intensity of $SiO_4C_7H_{17}^+$ to the calibration curve in Figure 4.13. The pressure was found to be $(7.7\pm0.3)\times10^{-7}$ Torr. With this, then, the rate constants were computed according to the development in Section 2.2 and are presented in Table 4.8 as well.

Two of the original six reactants decayed almost linearly as shown in Figure 4.19. This indicates a special imbalance between production and consumption

Ion	Time Constant (sec)	Rate Constant $\times 10^{-10}$ $cm^{-1}sec^{-1}$
$SiO_3C_5H_{13}^+$	0.064	6.25±0.02
$SiO_3C_6H_{15}^+$	0.095	4.21±0.01
$SiO_4C_6H_{15}^+$	0.063	6.35±0.02
$SiO_4C_8H_{20}^+$	0.070	5.71±0.01

Table 4.8. Reaction Rate Constants. With pressure known the reaction rate constants were calculated for the ions which showed exponential decay.

such that the species decay, but not exponentially. That is, if these two ions were only consumed, they would decay exponentially. If they were produced and consumed they might either grow, grow and then decay, or just decay. For a certain set of production and consumption coefficients, this decay might appear linear. Figure 4.20 shows the time evolution of three intermediate mass ions as they are produced and consumed. Initially their production dominates, but as their reactants decay, consumption takes over. And finally, Figure 4.21 displays the production of six heavy ions. On the time scale of this experiment it is not clear if they are final products or intermediaries for the production of heavier clusters.

This data now builds a reasonable picture for the system. Initially many ions are created by electron impact. At 15 eV, however, only six are created in any real abundance. In time they are allowed to react with each other and with the neutral TEOS background. These intermediate ions will be produced as the initial six are consumed. As their reactants run out, reactions between the intermediate ions and the neutral TEOS background will lead to the formation even heavier ions. There is no reason to expect this process to stop within the time frame of the experiment. Once the reactants for these heavier ions are consumed, reactions between these heavy clusters and the neutral TEOS background will take over and so on.

This cascade of forming heavier and heavier ions may be important for the use of TEOS in PECVD. After TEOS is fragmented in the reactor it will have time to

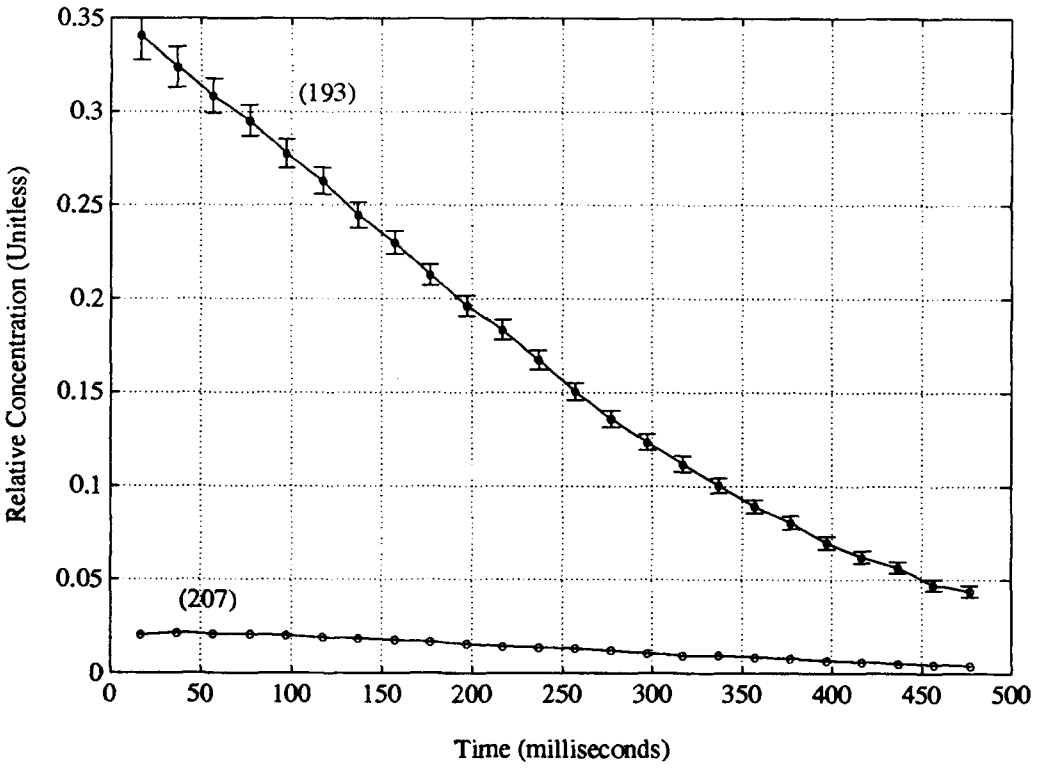

Figure 4.19. Decay Curves for $SiO_4C_7H_{17}^+$ and $SiO_4C_8H_{19}^+$. These ions seem to decay linearly in time indicating they are both produced and consumed.

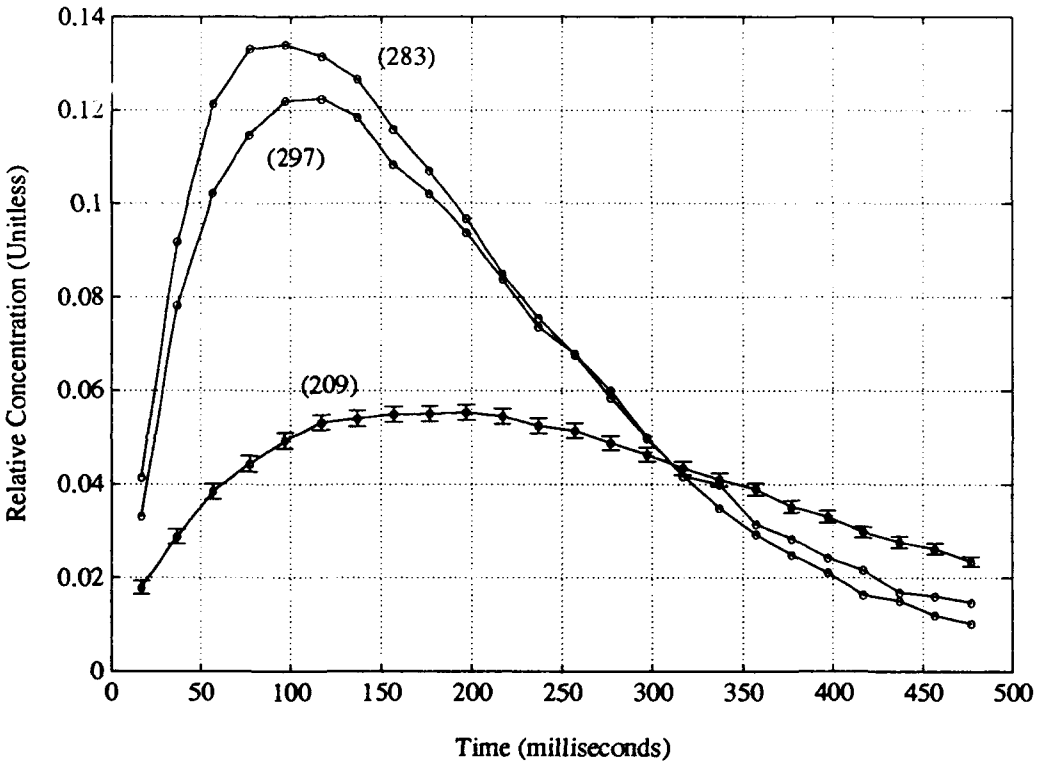

Figure 4.20. Production and Decay Curves for Masses 209, 283 and 297. These ions are produced and consumed.

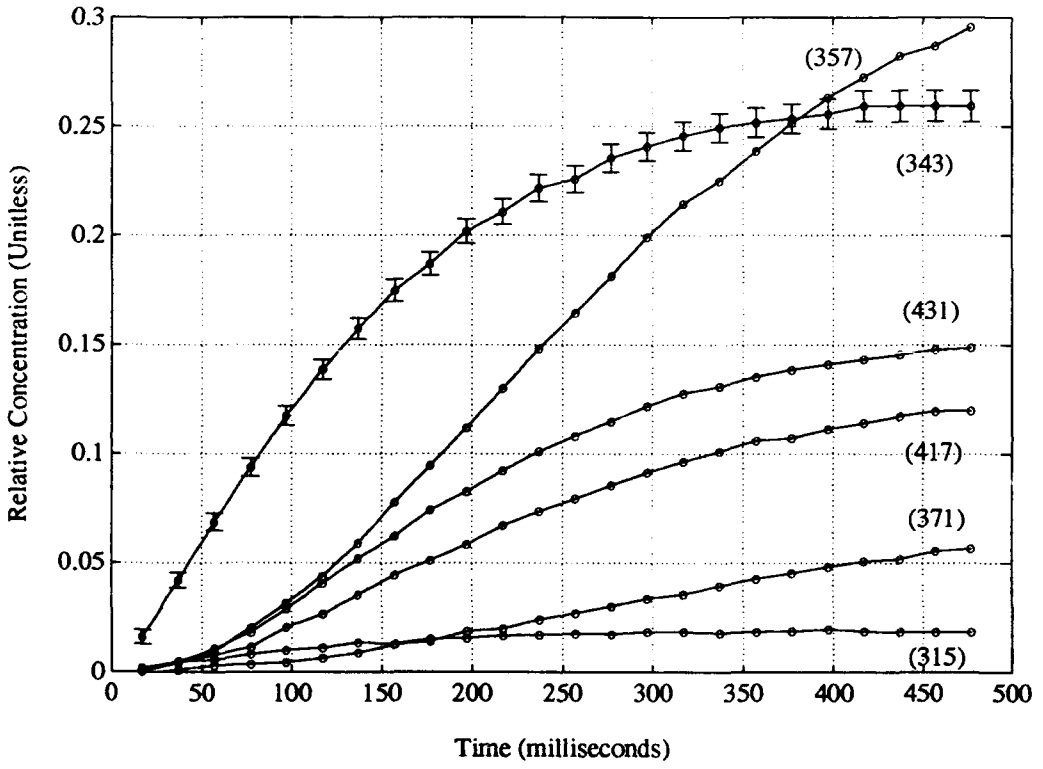

Figure 4.21. Production Curves for Masses 357, 343, 431, 417, 371 and 315. These ions are only produced on the time scale of this experiment.

react with neutral TEOS as ambipolar diffusion carries it to the walls. Since the heart of the TEOS molecule is silicon surrounded by four oxygens, it seems reasonable to suspect that the heavier ions may consist of $Si-O-Si$ cores surrounded by various arrangements of methoxy (OCH_3) and ethoxy (OC_2H_5). If this is so, then a network of $Si-O$ bonds is already starting to form before the ions strike the wall. Since TEOS is used for the deposition of SiO_2, this $Si-O$ bond chain could provide an important building block for the quartz film.

V. Concluding Remarks

In this thesis hopefully some of the ground work for understanding a TEOS plasma has been laid. Partial ionization cross-sections for 24 ions have been measured. 7 exhibited an unexpected resonance between threshold and 20 eV which appears to be associated with the breaking of a $Si - O$ bond. From these cross-sections some typical ionization rates were calculated assuming a Maxwellian energy distribution for the electrons. Then the ion chemistry was examined. Some species were observed to be consumed in time and their decay constants were measured. This lead to the formation of reactive intermediaries which were produced and consumed. Finally, the production of heavy clusters was observed.

For future work on TEOS there are still many questions to answer. The immediate need is to identify the heavy ions produced by ion chemistry. Also, the production of negative ions needs to be examined. This would help characterize the TEOS plasma more completely and give some insight into the ion chemistry.

Appendix A. *The Cross-Sections*

Listed here are the first 12 cross-sections of the 24 most abundant ions. The solid line is a plot of the parameterization according to Eq (4.1) and the coefficients from Table 4.6. For the curves with the unusual resonance, however, there is no parameterization.

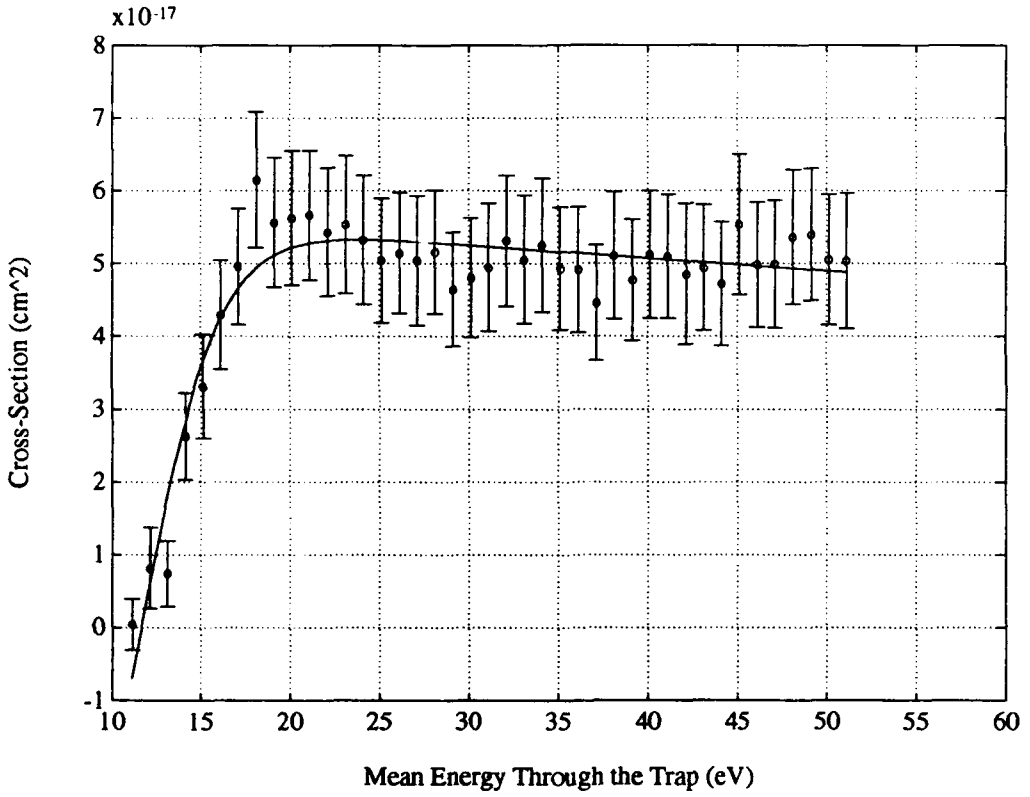

Figure A.1. $SiO_4C_8H_{20}^+$ Partial Ionization Cross-Section

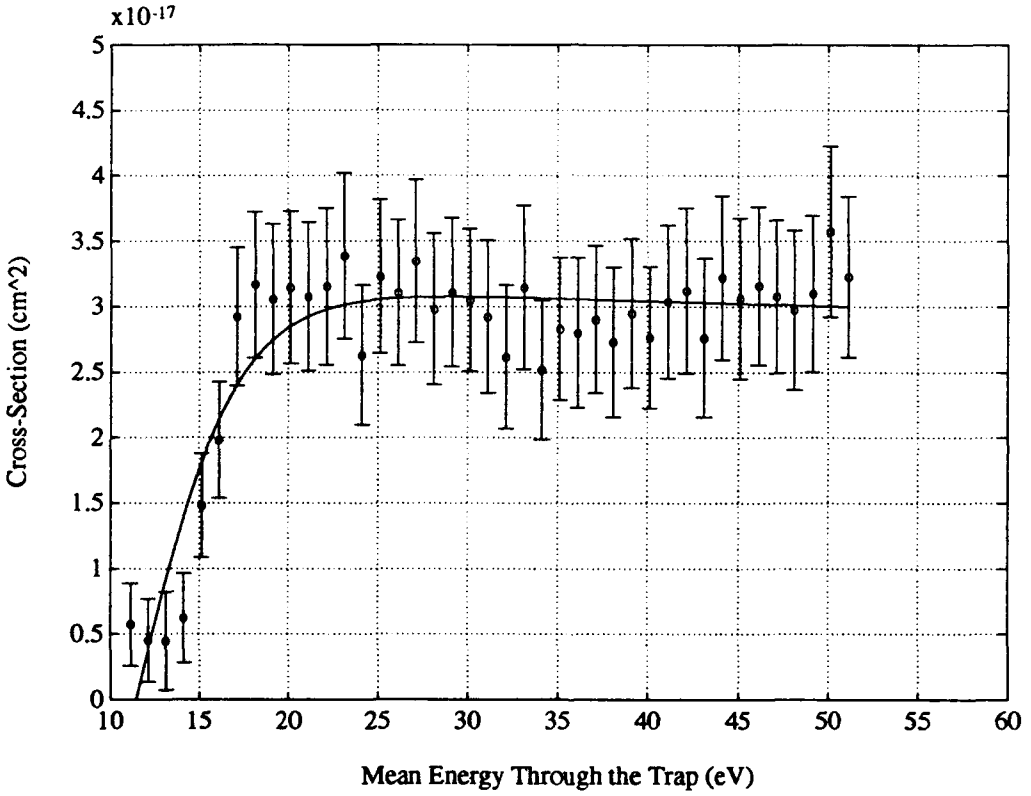

Figure A.2. $SiO_4C_8H_{19}^+$ Partial Ionization Cross-Section

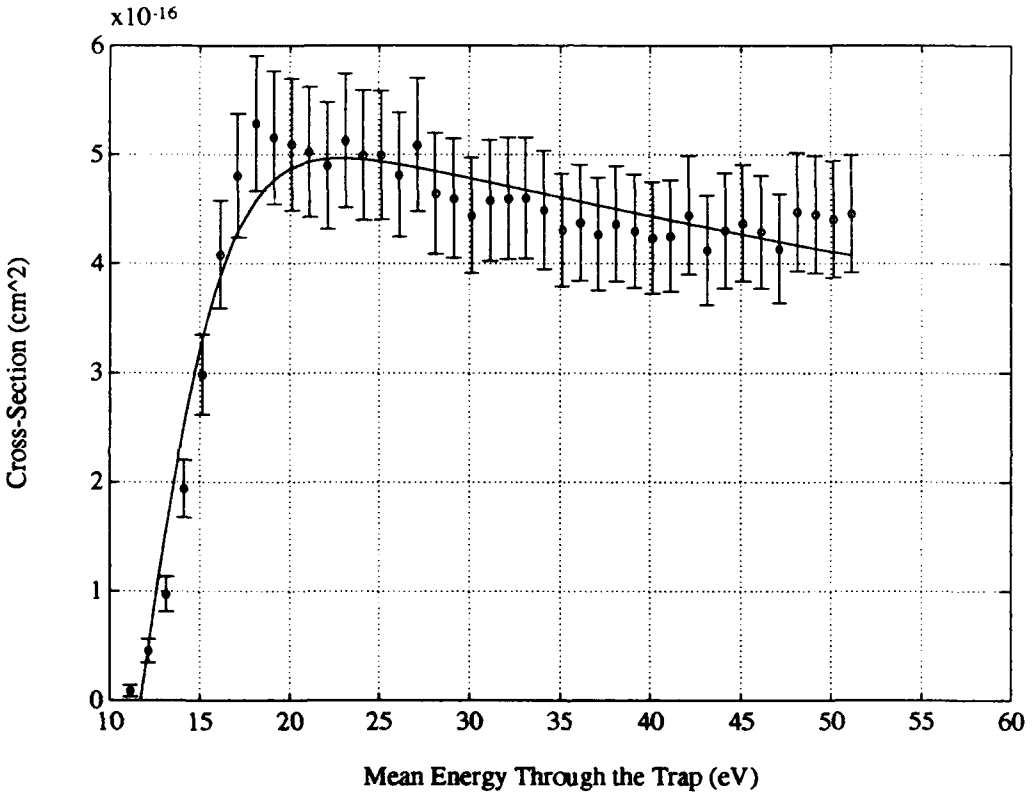

Figure A.3. $SiO_4C_7H_{17}^+$ Partial Ionization Cross-Section

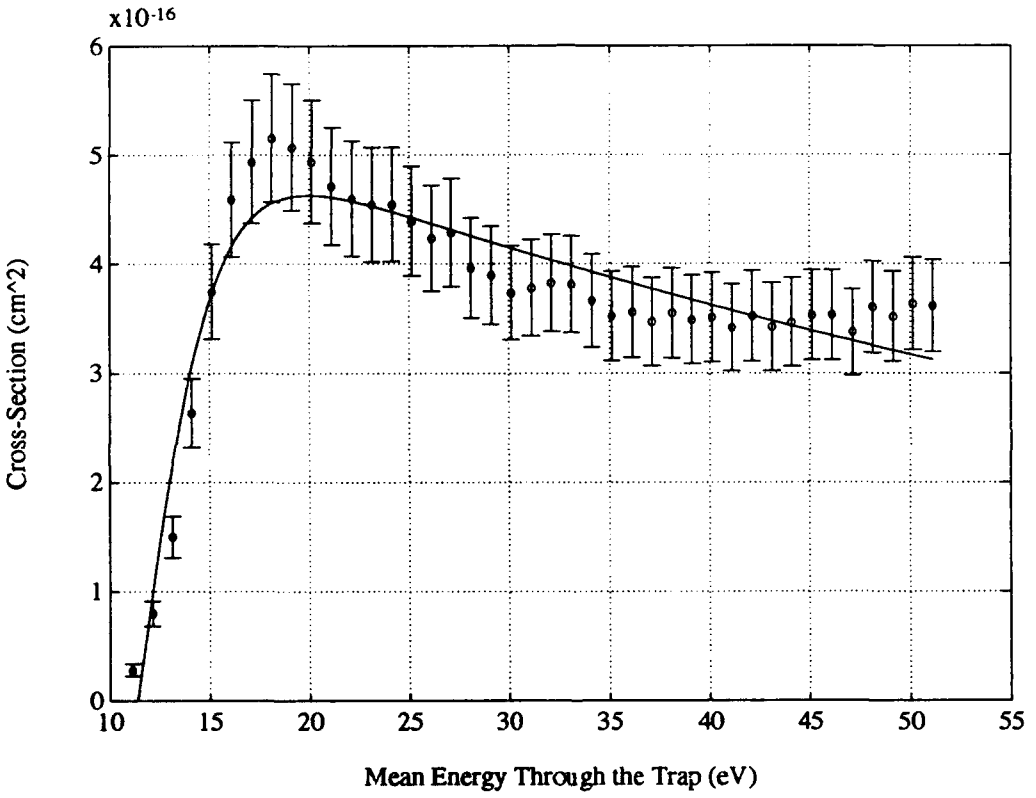

Figure A.4. $SiO_4C_6H_{15}^+$ Partial Ionization Cross-Section

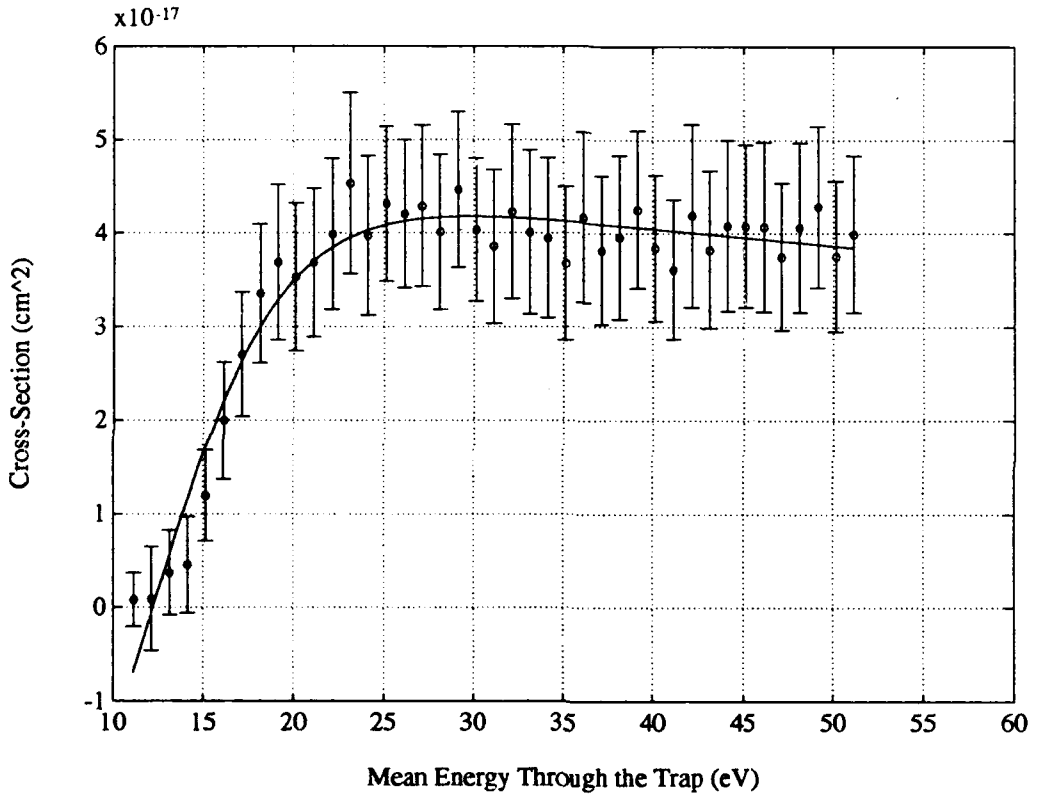

Figure A.5. $SiO_4C_5H_{13}^+$ Partial Ionization Cross-Section

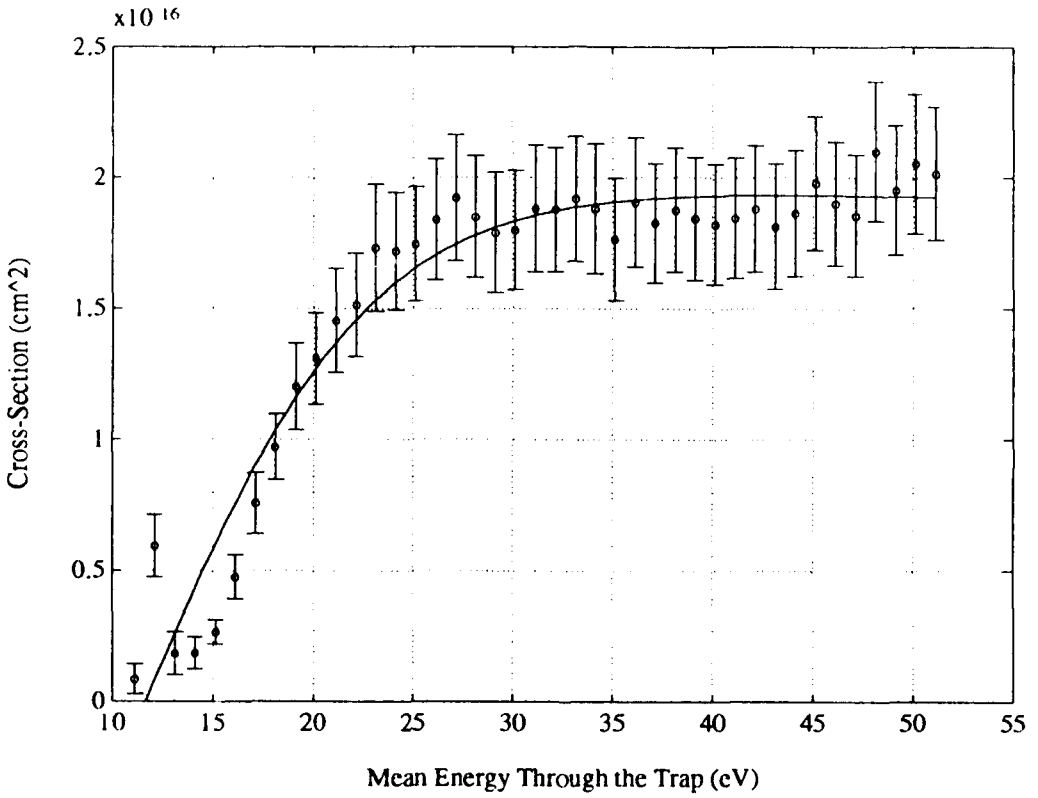

Figure A.6. $SiO_3C_6H_{15}^+$ Partial Ionization Cross-Section

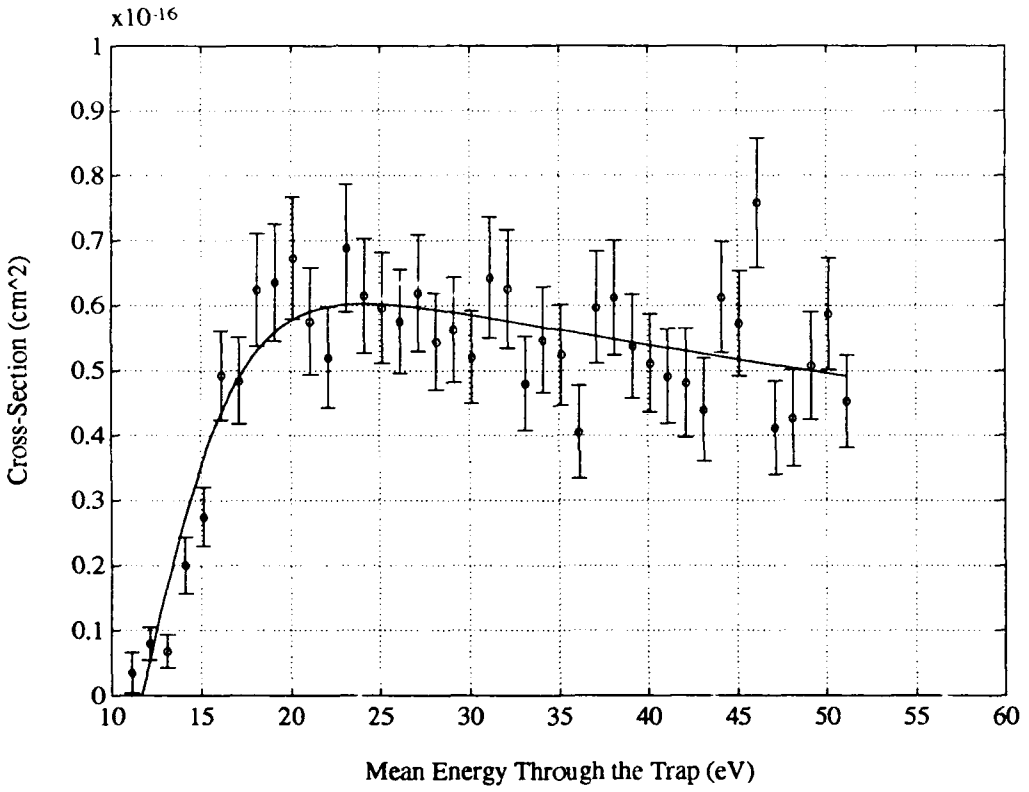

Figure A.7. $SiO_4C_4H_{11}^+$ Partial Ionization Cross-Section

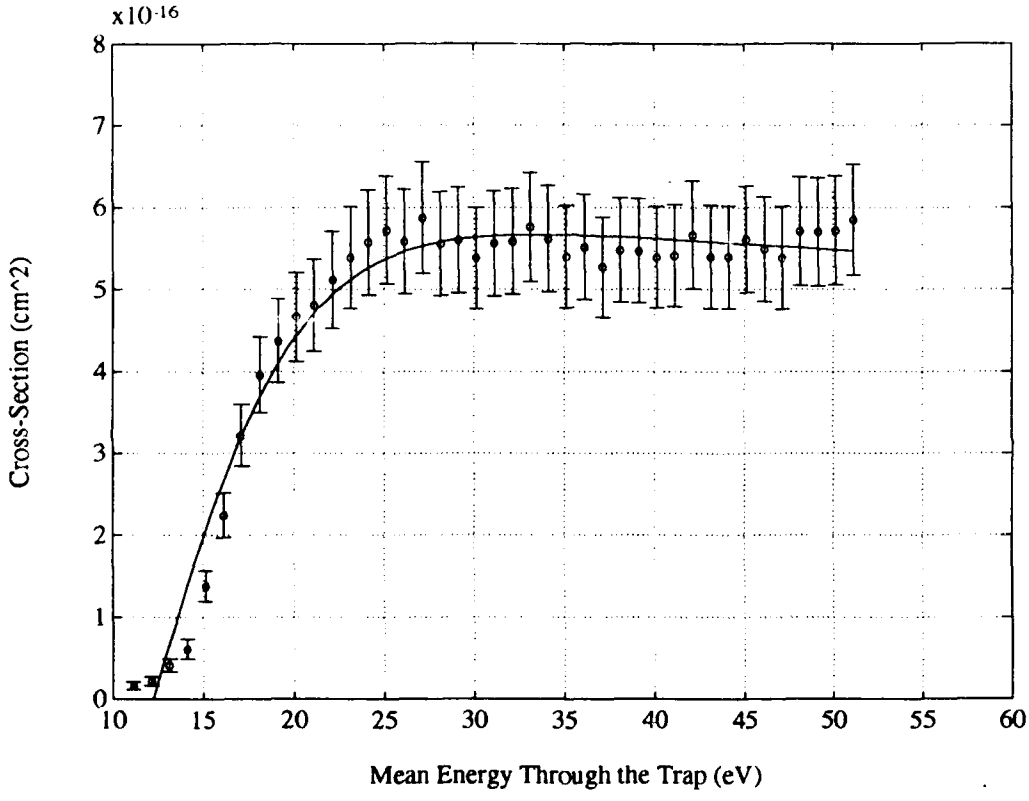

Figure A.8. $SiO_3C_5H_{13}^+$ Partial Ionization Cross-Section

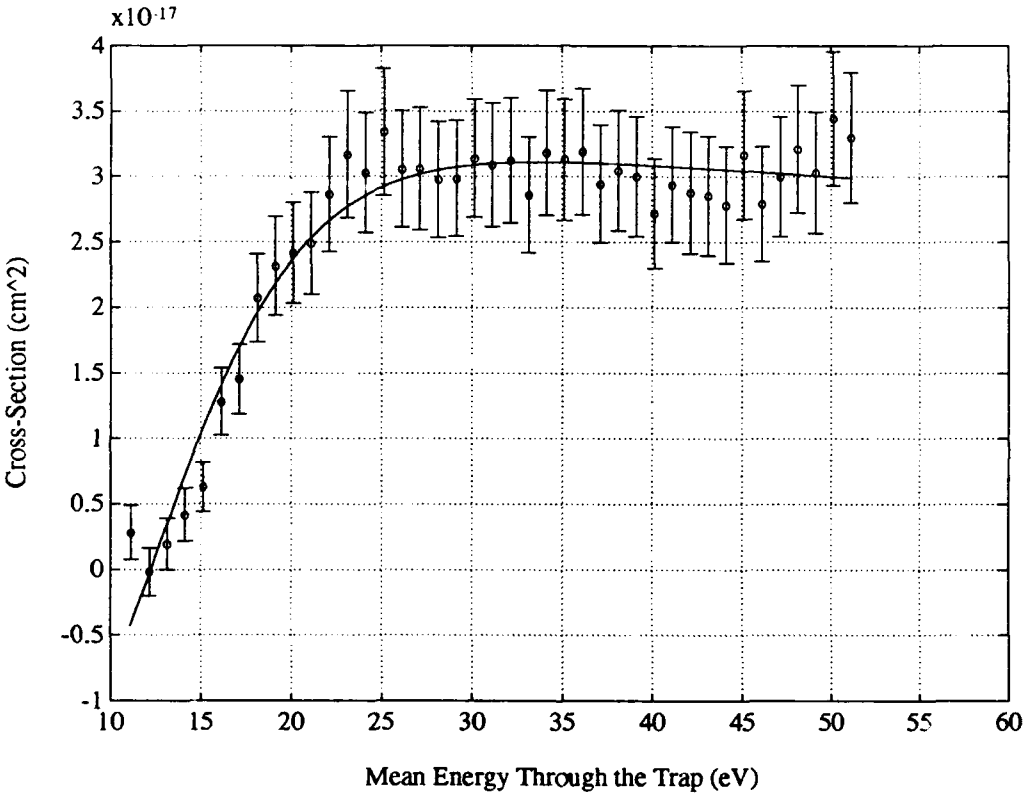

Figure A.9. $SiO_4C_3H_9^+$ Partial Ionization Cross-Section

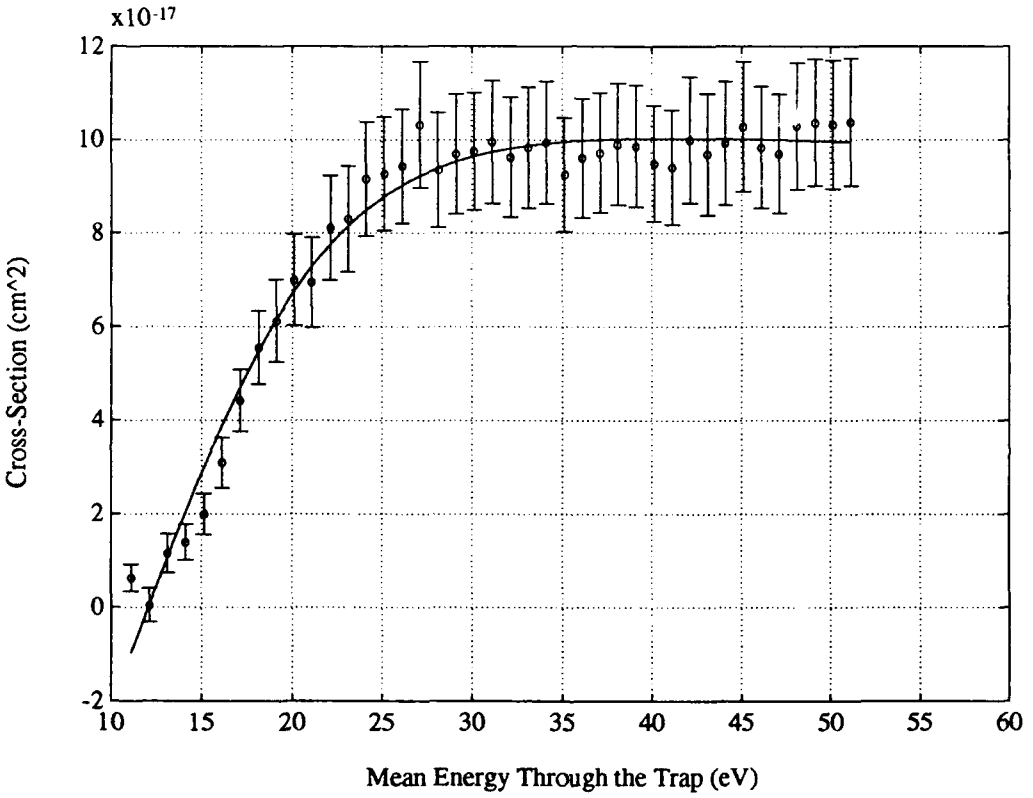

Figure A.10. $SiO_3C_4H_{11}^+$ Partial Ionization Cross-Section

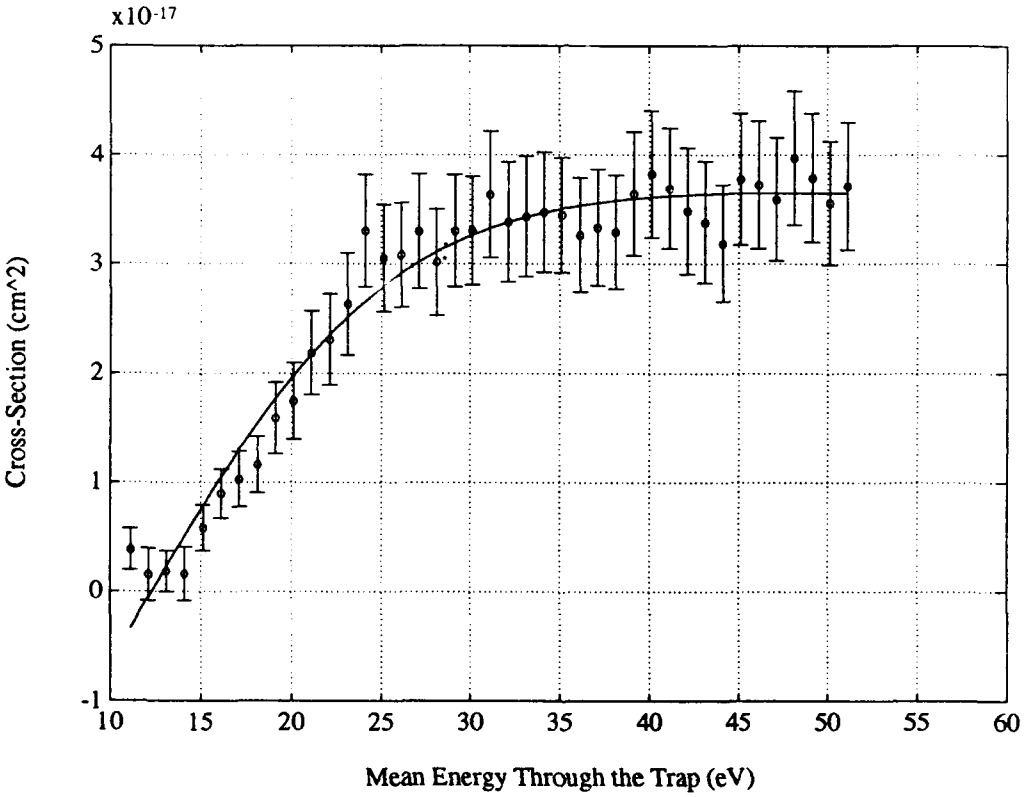

Figure A.11. $SiO_3C_3H_9^+$ Partial Ionization Cross-Section

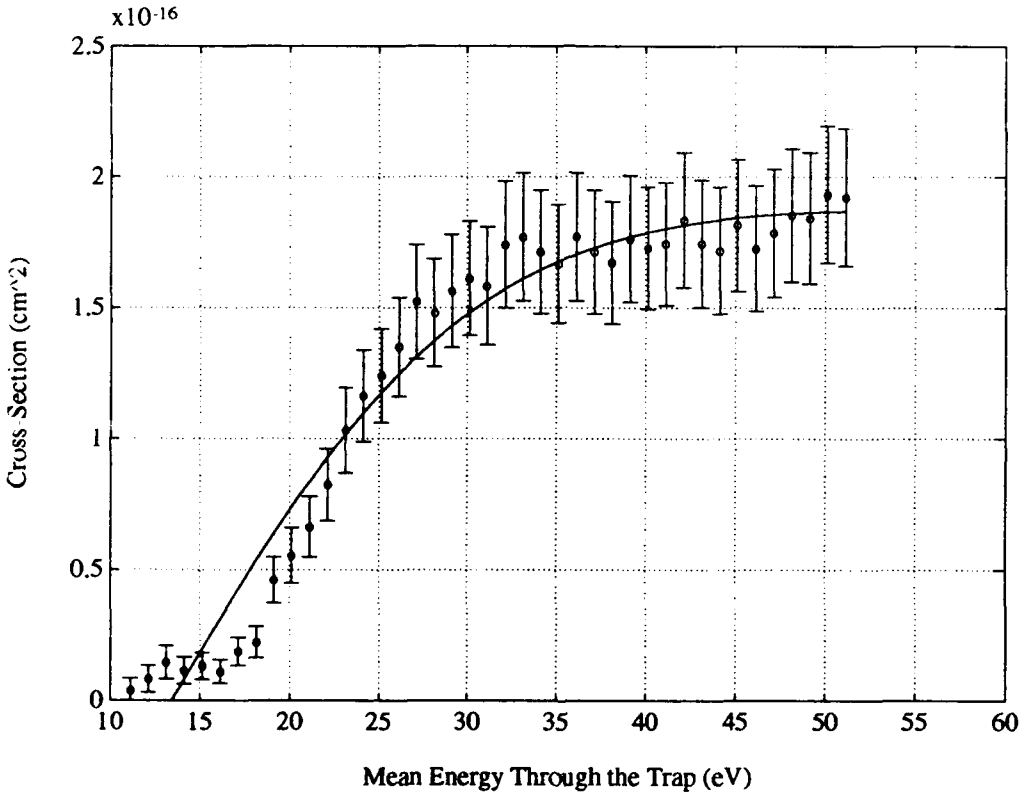

Figure A.12. $SiO_2C_4H_{11}^+$ Partial Ionization Cross-Section

Appendix B. *The Cross-Sections (Continued)*

Listed here are the last 12 cross-sections of the 24 most abundant ions. The solid line is a plot of the parameterization according to Eq (4.1) and the coefficients from Table 4.6. For the curves with the unusual resonance, however, there is no parameterization.

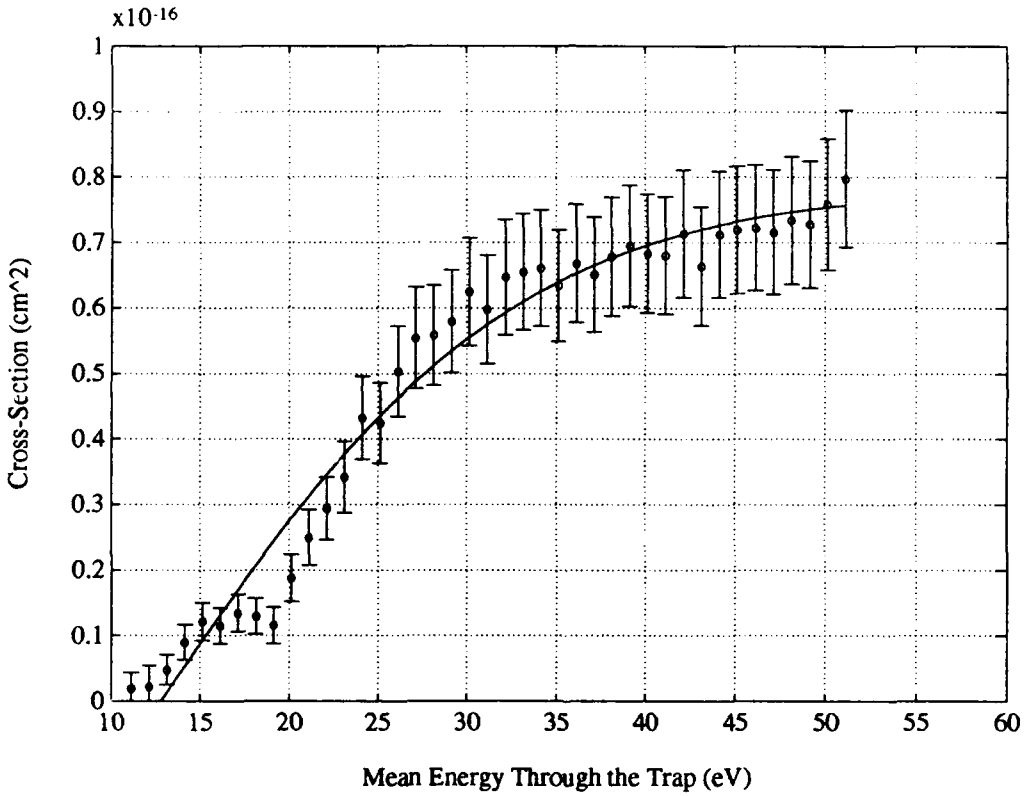

Figure B.1. $SiO_3C_2H_7^+$ Partial Ionization Cross-Section

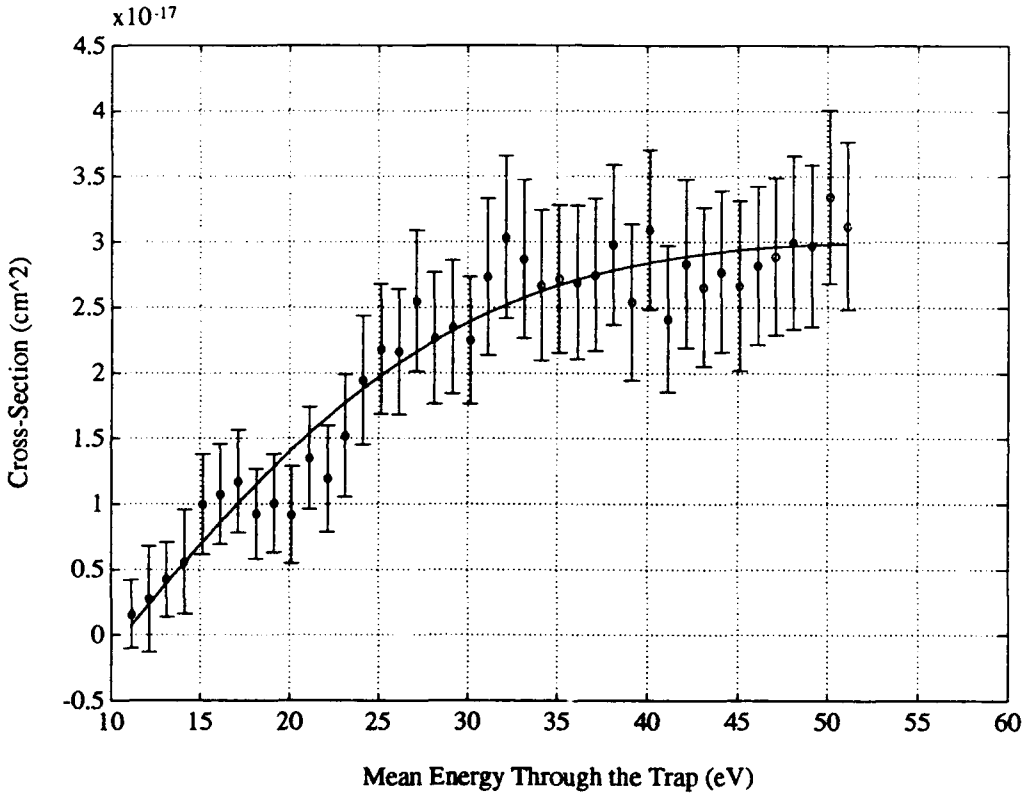

Figure B.2. $SiO_2C_3H_9^+$ Partial Ionization Cross-Section

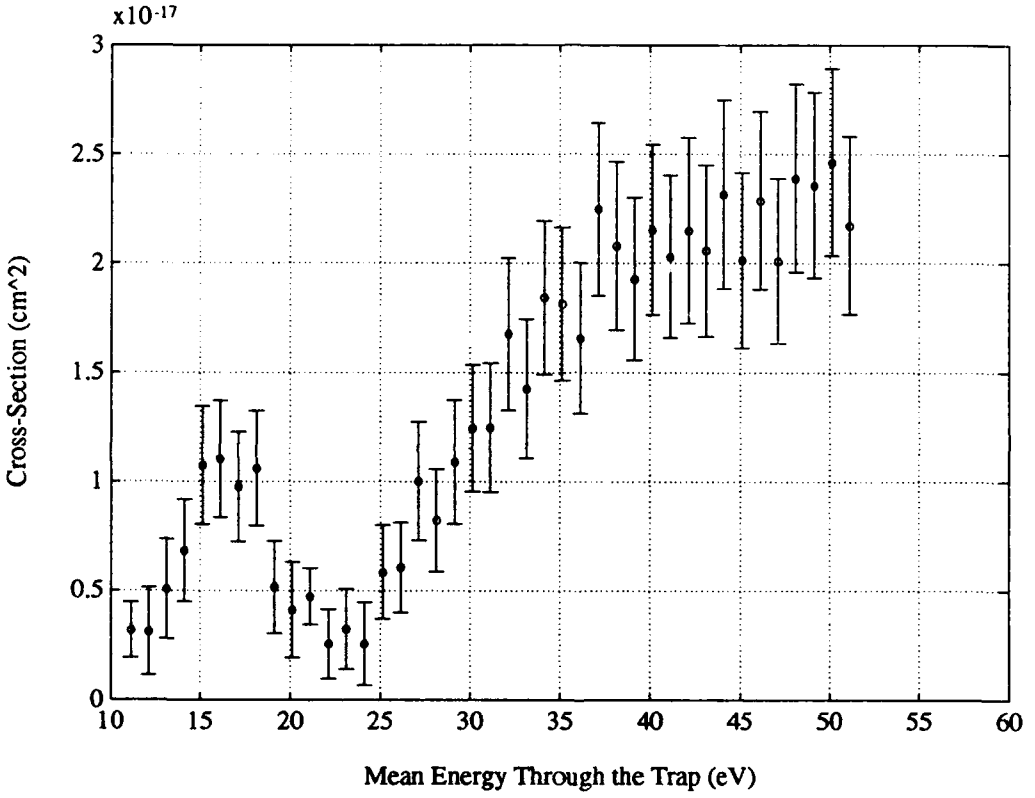

Figure B.3. $SiO_2C_3H_7^+$ Partial Ionization Cross-Section

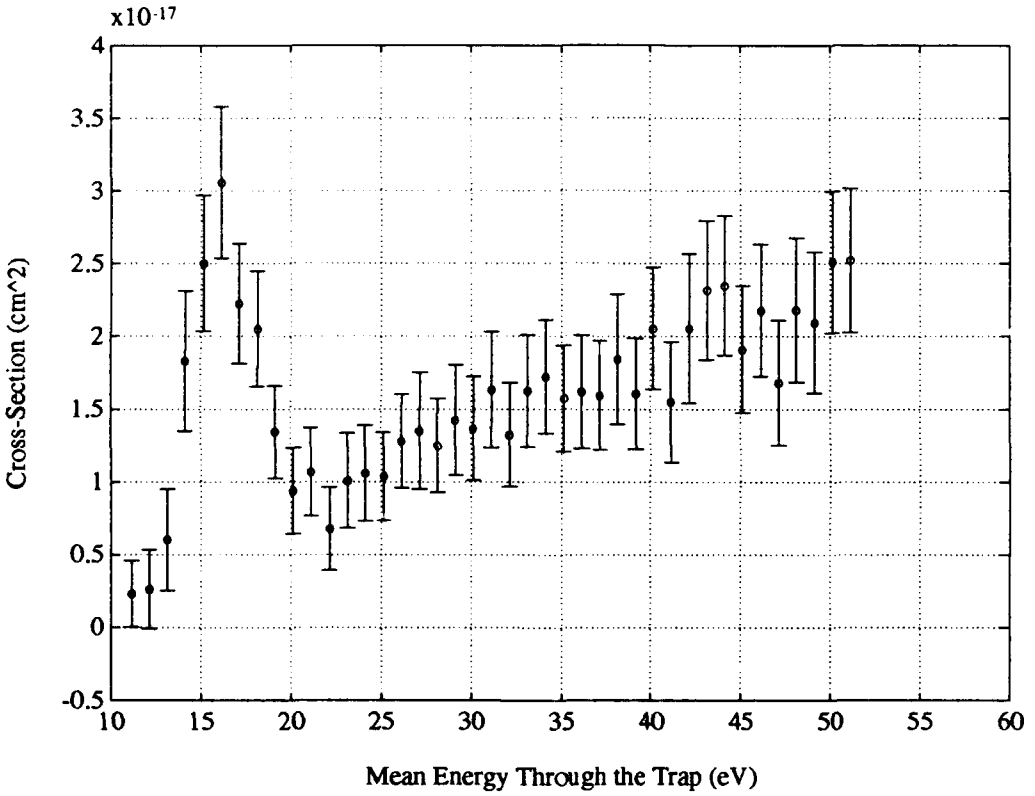

Figure B.4. $SiO_3CH_5^+$ Partial Ionization Cross-Section

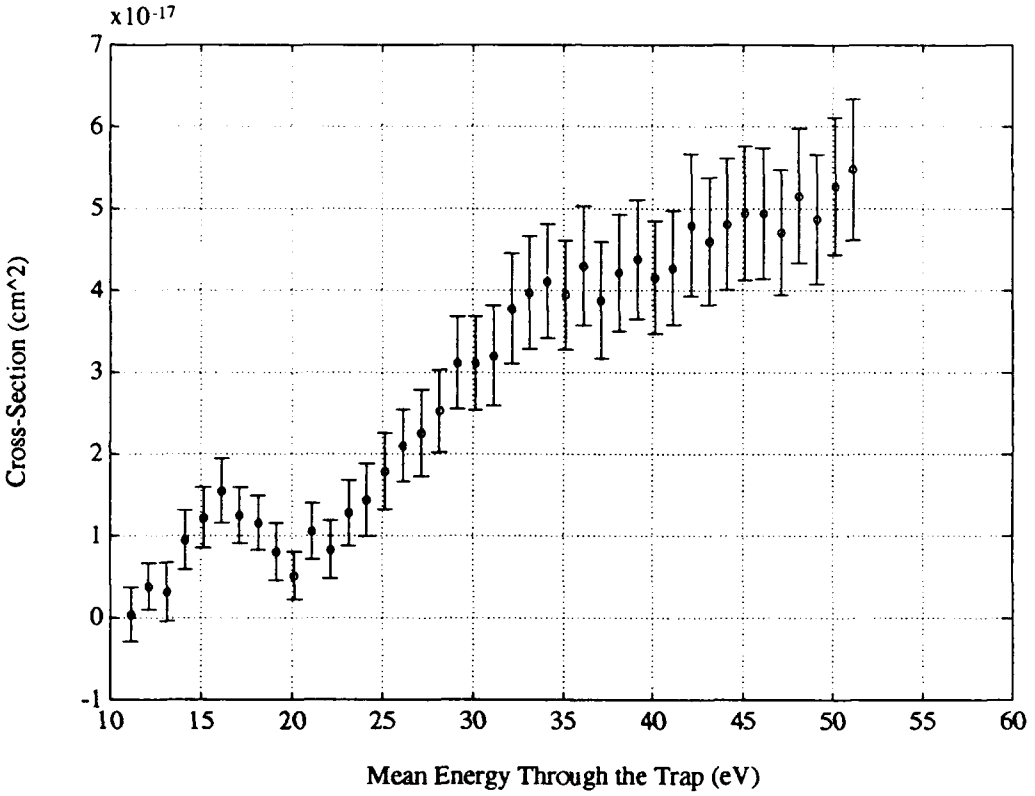

Figure B.5. $SiO_2C_2H_7^+$ Partial Ionization Cross-Section

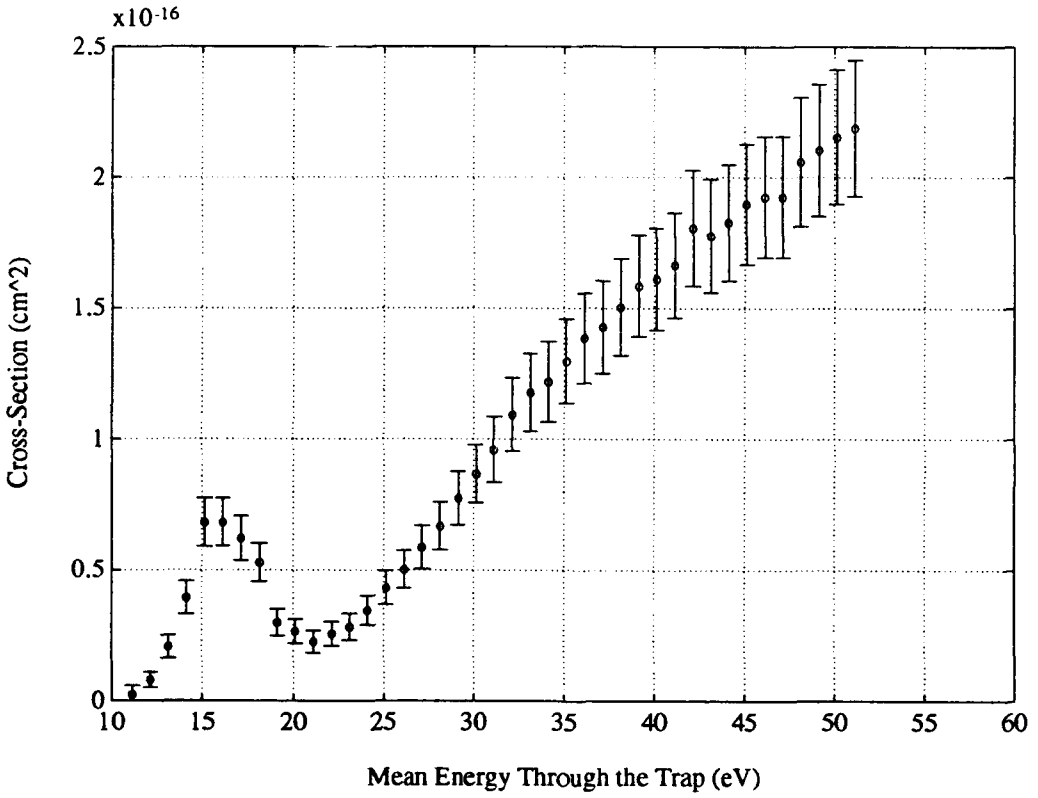

Figure B.6. $SiO_3H_3^+$ Partial Ionization Cross-Section

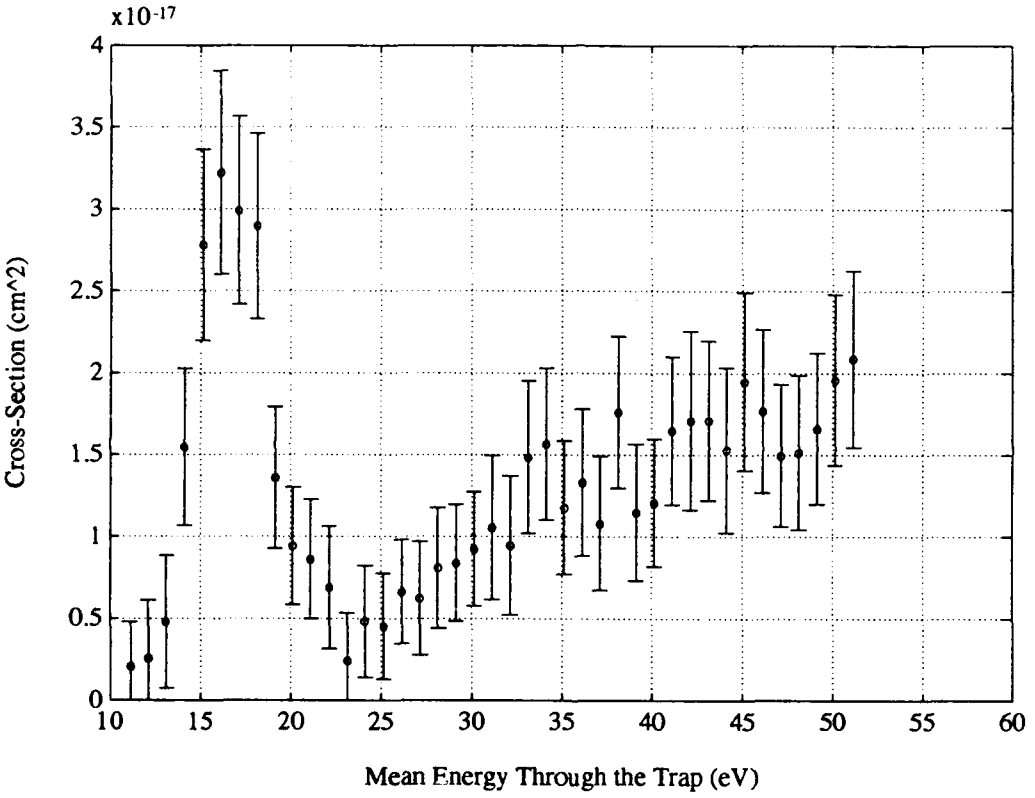

Figure B.7. $SiO_2CH_5^+$ Partial Ionization Cross-Section

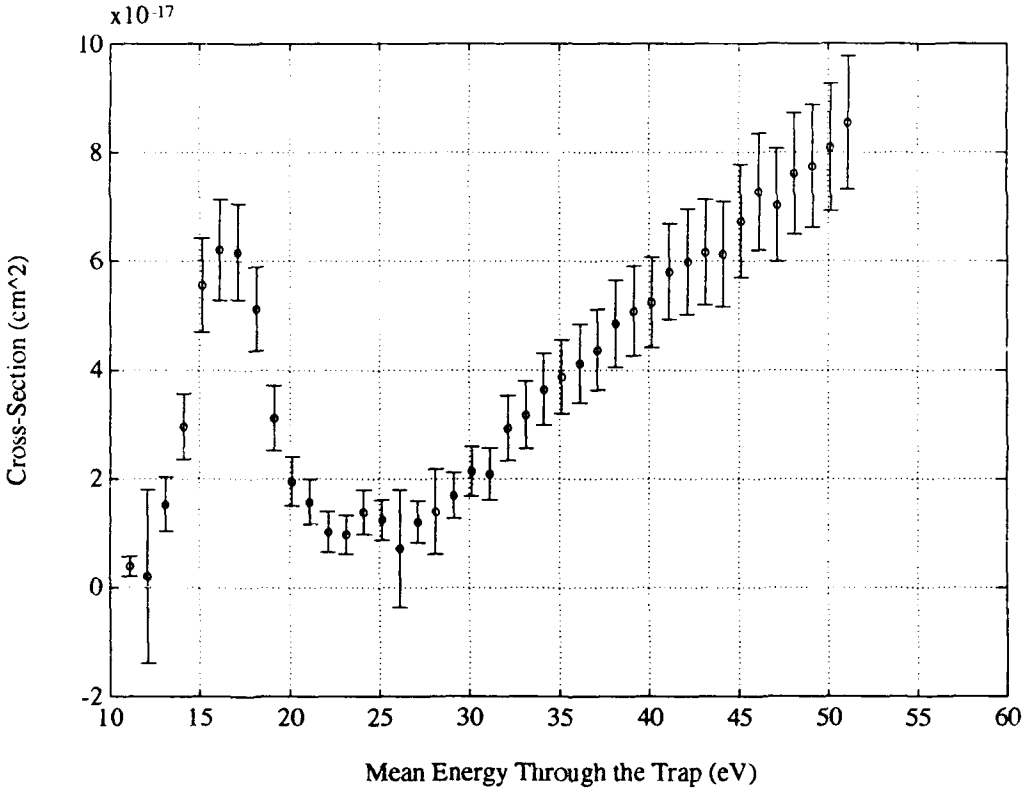

Figure B.8. $SiO_2H_3^+$ Partial Ionization Cross-Section

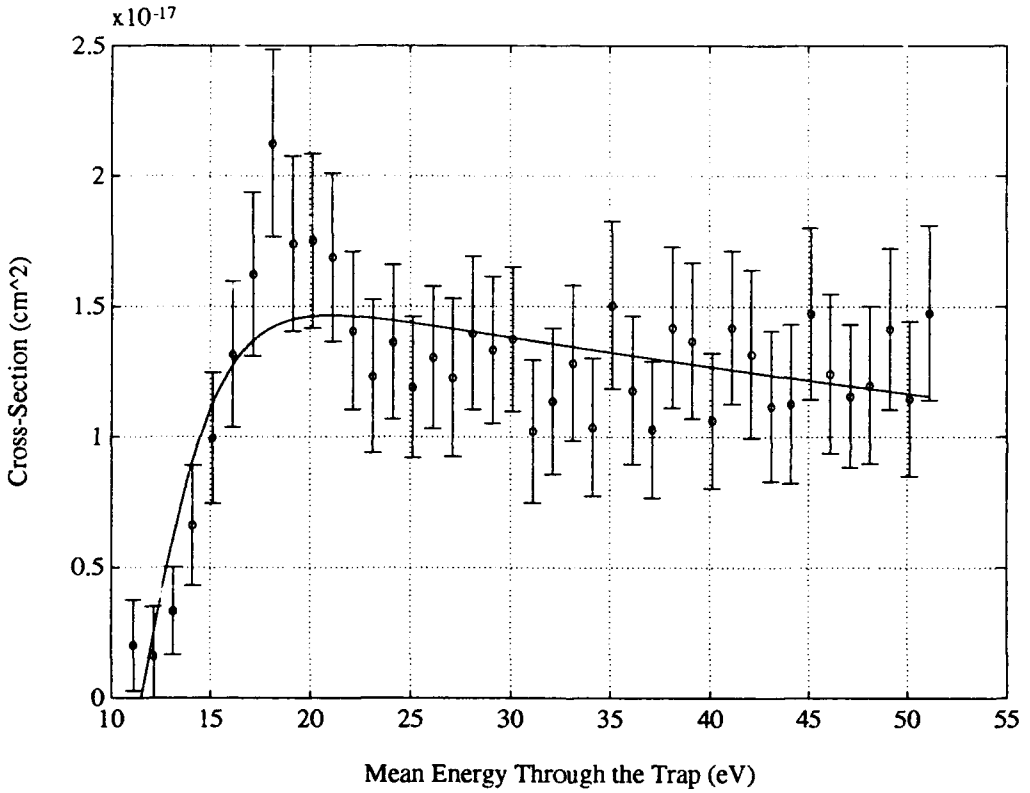

Figure B.9. $OC_2H_6^+$ Partial Ionization Cross-Section

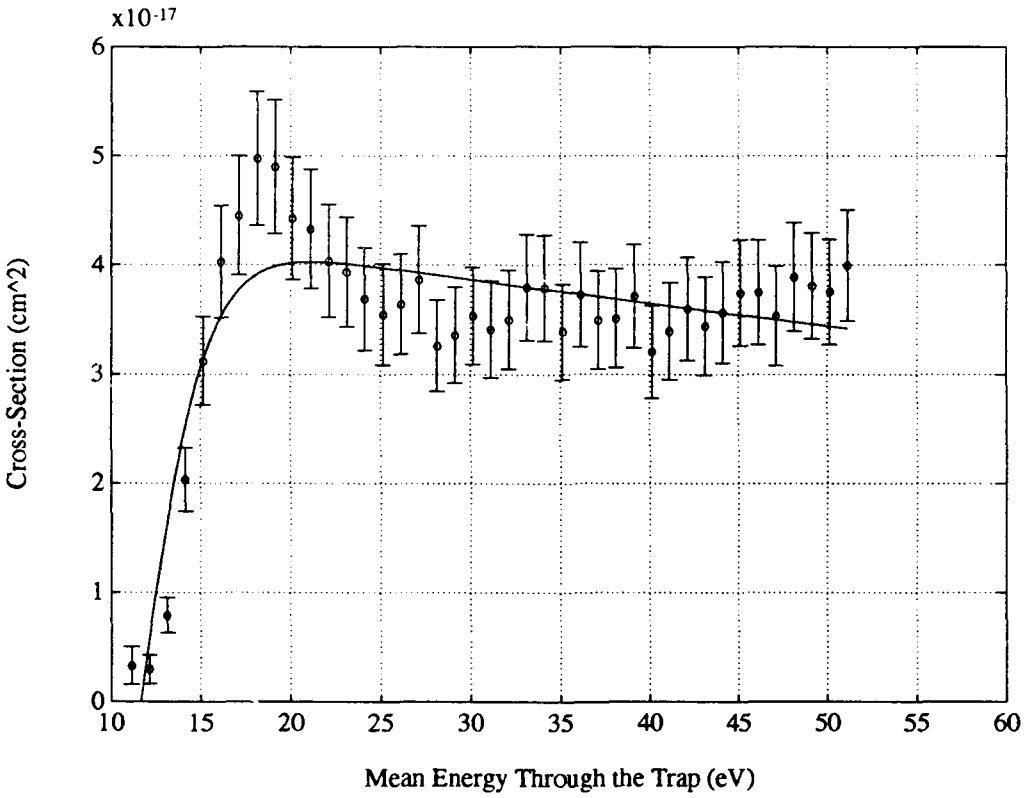

Figure B.10. $OC_2H_5^+$ Partial Ionization Cross-Section

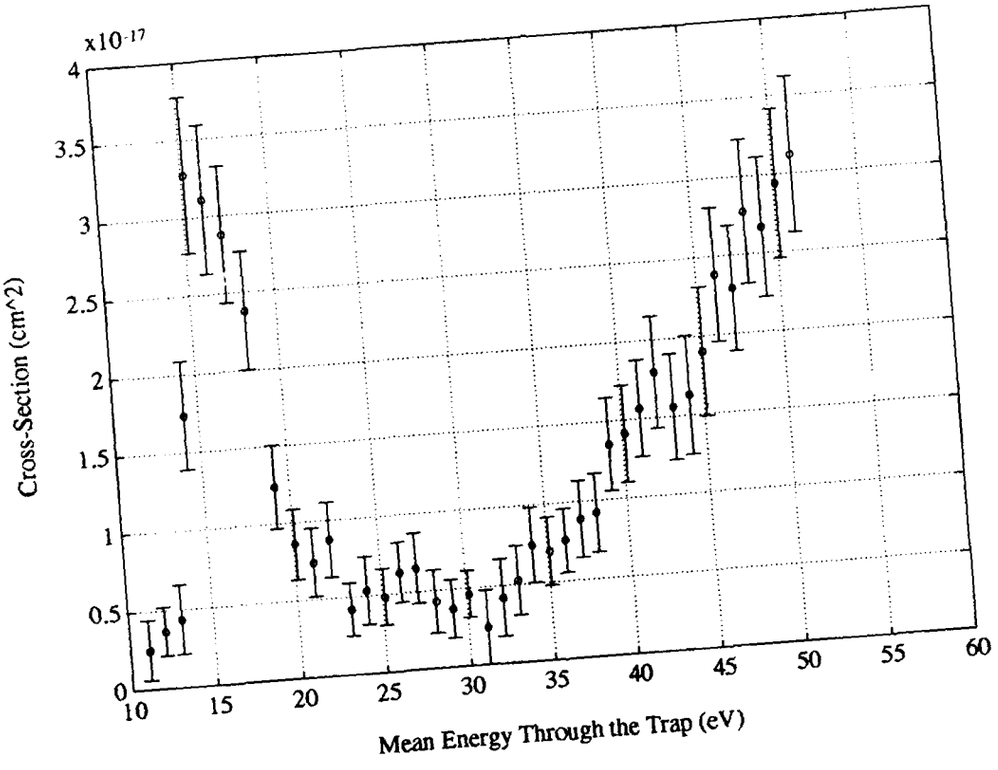

Figure B.11. $SiOH^+$ Partial Ionization Cross-Section

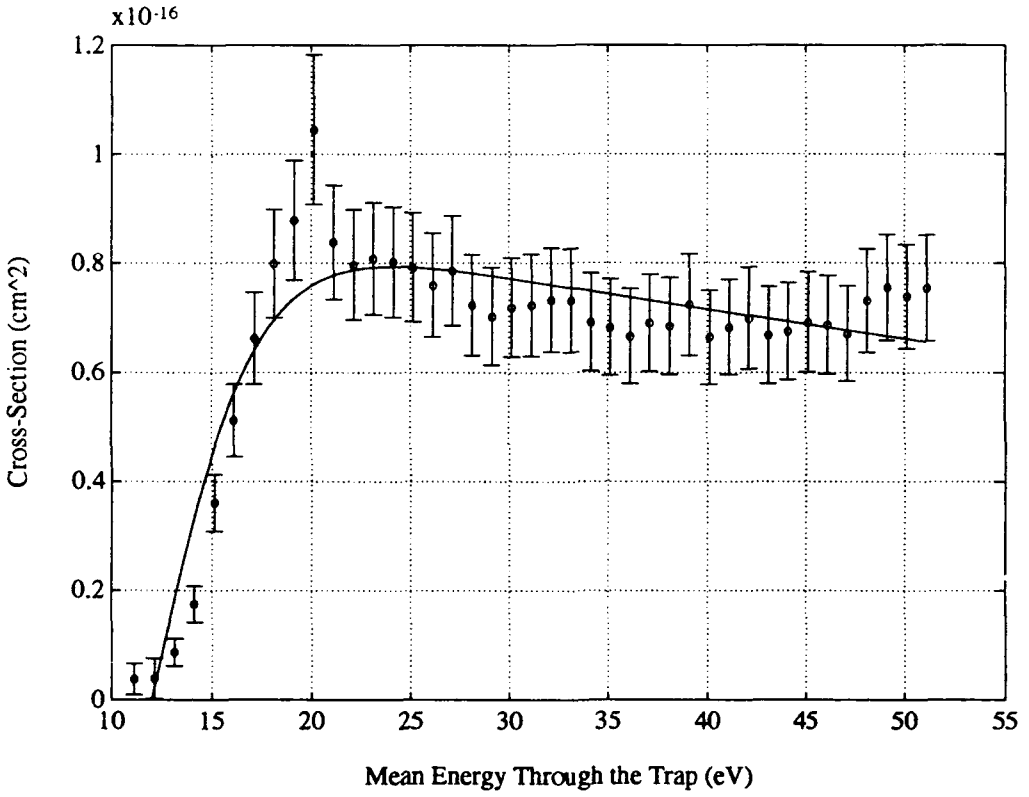

Figure B.12. OCH_3^+ Partial Ionization Cross-Section

Appendix C. *Data Reduction Details*

All the data was processed and reduced using MATLAB, a high-performance numerical computing evironment. The Fourier Transforms were accomplished using the built in FFT routine contained in the following code.

FTRAN.M:

```
function [f,xf,xm]=ftran(t,zerofill,nyqfreq)

% [f,xf,xm]=ftran(t,zerofill,nyqfreq)
%
% t        = time domain data (V)
% zerofill = size of total transform
% nyqfreq  = Nyquist frequency for data (Hz)
%
% This function performs a zero-filled Fourier Transform, while
% establishing the x-axis arrays for frequency and mass.  This
% frequency to mass transformation incorporates the latest
% calibration parameters.
%
% f  = Fourier Transformed time domain data (V/Hz)
% xf = frequency array (Hz)
% xm = mass array according to a0, b0, and c0 (a.m.u.)

if zerofill<length(t)
   zerofill=length(t)
end
offset=mean(t)
f=abs(fft(t-offset,zerofill))/(2*nyqfreq);
halflength=round(zerofill/2);
f=f(1:halflength);
xf=(0:halflength-1)*nyqfreq/halflength;
a0=9.264399624519356e+14;
b0=-1.111021829758421e+10;
c0=-3.661395130390922e+06;
xm=(2*(c0-xf.^2)).\(-b0-sqrt(b0^2-4*a0*(c0-xf.^2)));
xm(1)=1e7;
```

The transforms were generally zerofilled to the next radix two number above twice the number of data points taken. Also, the average value of the data was subtracted from the entire data set first to eliminate any Fourier components associated with the step above the baseline.

After taking the Fourier Transform of the data it was divided by the gain curve shown in Figure C.1 associated with the amplifier. This curve was measured by Riehl experimentally [16:A-17]. Outside the regions depicted (the bandwidth) the curves explode to infinity.

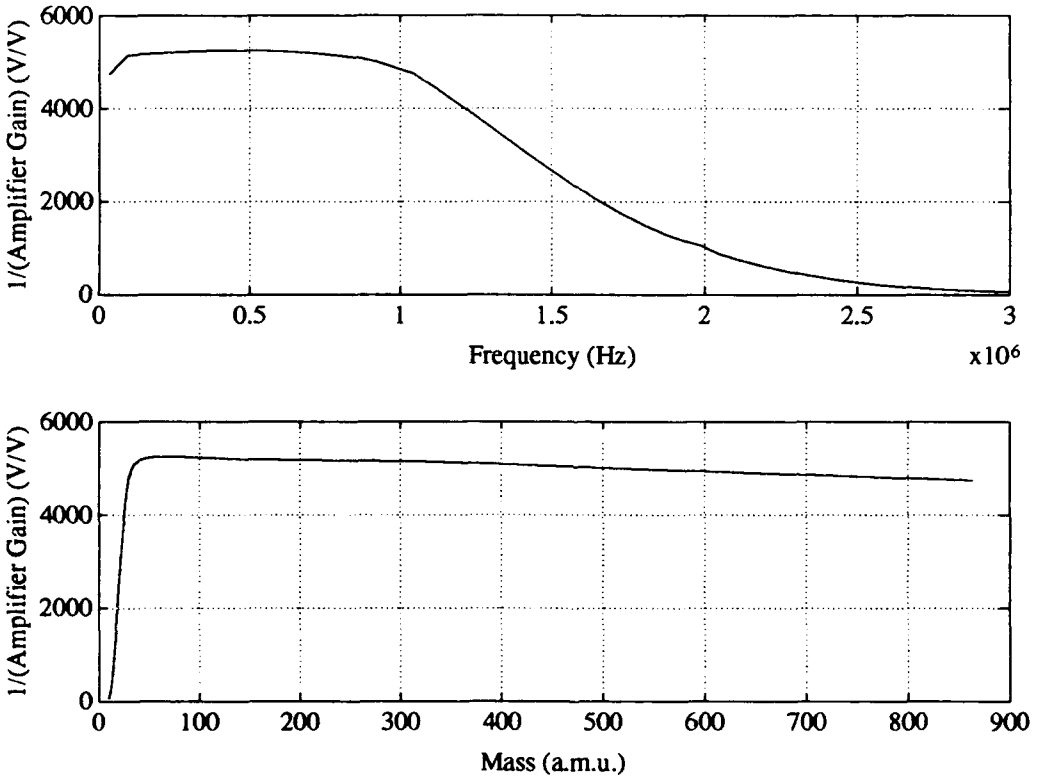

Figure C.1. Amplifier Gain Curve. In the frequency domain (upper plot) this curve is presented up to 5 MHz and in the mass domain (lower plot) down to 6.1 a.m.u.

The mass spectrum was analyzed with the function listed next. The overall idea is to input a mass spectrum, some error parameters, and a peak magnitude.

The code then searches the data for all peaks greater than the peak magnitude given by the user and outputs two lists. One is a complete characterization of each peak. It gives the peak height, frequency, and mass (according to the transformation parameters determined by a calibration) along with uncertainties for each quantity. The second list is a comparison of the first list to a database containing all possible combinations of the TEOS constituant atoms. For each mass and mass uncertainty the routine looks for atomic combinations possible within that mass and range. Of course some of these combinations are not chemically plausible, but that is for the user to decide.

CANONICAL.M:

```
function  [all1,all2]=canonical(grt,nb,gain,xf,f,fb)

% [all1,all2]=canonical(grt,nb,gain,xf,f,fb)
%
% grt  = peaks greater than this value (V/Hz)
% nb   = number of bits used on the oscilloscope (out of 8)
% gain = the gain curve (V/V)
% xf   = frequency vector (Hz)
% f    = Fourier Transformed (and gain adjusted) data (V/Hz)
% fb   = Fourier Transformed (and gain adjusted) background (V/Hz)
%
% This function searches for peaks in a TEOS mass spectrum,
% characterizes them, and returns possible combinations of
% TEOS constituant atoms which could account for the peak.
%
% all1(:,1:2) = peak height and uncertainty (V/Hz)
% all1(:,3:4) = frequency and uncertainty (Hz)
% all1(:,5:6) = mass and uncertainty (a.m.u.)
%
% all2 = Alternates rows.  For "<mass> 0 0 0 0" the mass is an
%        experimentally measured peak.  For "# # # # <mass>" the
%        first for #s are the numbers of Si, O, C, and H present
%        in theoretical mass <mass>.  This combination falls
%        within the error of the experimentally determined mass
%        above.

table=zeros(1890,5);
```

```
tablesort=zeros(1890,5);

% This section generates a matrix of all possible combinations
% of 1 Si, 4 O, 8 C, and 20 H found in TEOS.  The matrix is
% then sorted into order of lowest to highest mass in a variable
% called "tablesort".

i=1;
for Si=0:1
   for O=0:4
       for C=0:8
           for H=0:20
              mass=27.976927*Si+15.994915*O+12.000000*C+
                   1.007825*H-0.0005486;
              table(i,:)=[Si O C H mass];
              i=i+1;
           end
       end
   end
end
[masssort,n]=sort(table(:,5));
for a=1:1890
    tablesort(a,:)=table(n(a),:);
end

% This second section then processes the data (xf,f)
% according to the "grt" parameter.  The output, "all1", is a
% table of each peak magnitude, its exact frequency, associated
% mass, and mass uncertainty.

a0=9.264399624519356e+14;          % Quadratic conversion
b0=-1.111021829758421e+10;         % coefficients.
c0=-3.661395130390922e+06;         %
da0=0;                             % Quadratic conversion factor
db0=0;                             % uncertainties.
dc0=0;                             %
tgt=find(f>grt);                   % Indices of data above "grt".
i=1;                               % This routine determines
for a=2:length(tgt)                % the beginning and ending
if tgt(a)-tgt(a-1) ~= 1            % indices of each peak set.
       stp(i)=a-1;                 %
       i=i+1;                      %
```

```
        stp(i)=a;                    %
        i=i+1;                       %
     end                             %
end                                  %
stp=[1 stp length(tgt)];             %
tgte=tgt(stp);                       %

i=1;                                          % This routine seeks
for a=1:2:length(tgte)                        % out the full width
   [y,j]=max(f(tgte(a):tgte(a+1)));           % half max of the
       for b=1:500                            % peak determining
          if f(j-1+tgte(a)-b)<=y/2            % the uncertainty in
             fwhml=xf(j-1+tgte(a)-b);         % the frequency and
             break                            % hence the
           end                                % uncertainty in
       end                                    % the mass.
       for b = 1:500                          %
          if f(j-1+tgte(a)+b)< y/2            %
             fwhmr=xf(j-1+tgte(a)+b);         %
             break                            %
          end                                 %
       end                                    %
                                              %
   all1(i,4)=(fwhmr-fwhml)/2;                 % Peak uncertainty.
   dxf=(fwhmr-fwhml)/2;                       % Dummy variable.
   ind1=j-2+tgte(a);        % Indices of the three points at
   ind2=j-1+tgte(a);        % the tip of the peak.
   ind3=j+tgte(a);          %

   % This subroutine fits a quadratic to the three highest
   % points in the peak and, using differential calculus,
   % determines at what frequency the peak occurs and
   % the magnitude of the peak.

   temp1=max(xf(ind1:ind3))\xf(ind1:ind3);
   temp2=max(f(ind1:ind3))\f(ind1:ind3);
   fit=polyfit(temp1,temp2',2);
   all1(i,3)=max(xf(ind1:ind3))*(-fit(2)/(2*fit(1)));

   % This subroutine determines the total error in the peak
   % height.  It accounts for background noise, gain
   % uncertainty, and digitizer uncertainty.
```

```
   k=find(xf>all1(i,3)-dxf & xf<all1(i,3)+dxf);
   df1=mean(fb(k));                    % Background noise avg.
   df2=gain(ind2)\f(ind2)*(2^(-nb-1)); % Digitizer uncertainty.
   df3=gain(ind2)^2\f(ind2)*50;        % Gain uncertainty.
   all1(i,2)=df1+abs(df2-df3);
   all1(i,1)=max(f(ind1:ind3))*
             polyval(fit,(-fit(2)/(2*fit(1))))-df1;

   % With the frequency known, the conversion to mass is made.

   all1(i,5)=(2*(c0-all1(i,3).^2)).\
             (-b0-sqrt(b0^2-4*a0*(c0-all1(i,3).^2)));

   % With the frequency uncertainty known, the conversion to
   % mass uncertainty is made.

   u1=2*c0^2*da0-b0*c0*db0+b0^2*dc0-2*a0*c0*dc0-2*b0^2*dxf.*
      all1(i,3);
   u2=4*a0*c0*dxf.*all1(i,3)-4*c0*da0*all1(i,3).^2+
      b0*db0*all1(i,3).^2;
   u3=2*a0*dc0*all1(i,3).^2-4*a0.*dxf.*all1(i,3).^3;
   u4=2*da0*all1(i,3).^4-c0*db0*sqrt(b0^2-4*a0*c0+4*a0.*
      all1(i,3).^2);
   u5=b0*dc0*sqrt(b0^2-4*a0*c0+4*a0*all1(i,3).^2);
   u6=2*b0*dxf.*all1(i,3).*
      sqrt(b0^2-4*a0*c0+4*a0*all1(i,3).^2);
   u7=db0*(all1(i,3).^2).*
      sqrt(b0^2-4*a0*c0+4*a0*all1(i,3).^2);
   u8=2*((c0-all1(i,3).^2).^2).*
      sqrt(b0^2-4*a0*c0+4*a0*all1(i,3).^2);
   all1(i,6)=abs(u8.\(u1+u2+u3+u4+u5-u6+u7));

   if all1(i,4)>=60;              % This little part makes the
      i=i-1;                      % program skip peaks wider than
   end                            % 120 Hz.

   i=i+1;                         % Advance the index.

end

% And finally, this section examines the data in the second
```

```
% section, compares to the first section, and for each measured
% mass and uncertainty gives the possibilities.

for a=1:length(all1)
    temp1=all1(a,5)+all1(a,6);
    temp2=all1(a,5)-all1(a,6);
    temp3=tablesort(:,5);
    pssbts=find(temp3<=temp1 & temp3>=temp2);
    data=all1(a,5);
    theory=tablesort(pssbts,:);
    all2=[all2
          data 0 0 0 0
          theory
          ];
end
```

Once the peaks were identified the following code was developed to measure the height of each peak and the area under it. Again the user inputs the spectrum with some error parameters. This time a mass range is specified. The routine finds the peak within that range and reports the quantities mentioned along with their uncertainties.

YPEAK.M:

```
function  all=ypeak(xml,xmh,nb,gain,chg,chgb,xf,xm,f,fb)

% all=ypeak(xml,xmh,nb,gain,chg,chgb,xf,xm,f,fb)
%
% xml  = lower mass boundary (a.m.u.)
% xmh  = higher mass boundary (a.m.u.)
% nb   = number of bits used on the oscilloscope
%        (out of 8)
% gain = the gain curve (V/V)
% chg  = the total charge passing through the plasma (C)
% chgb = the total charge passing through the plasma
%        background (C)
% xf   = frequency array (Hz)
% xm   = mass array (a.m.u.)
% f    = Fourier Transformed (and gain adjusted) data
%        (V/Hz)
```

```
% fb   = Fourier Transformed (and gain adjusted) background
%        data (V/Hz)
%
% This function searches for a peak in the mass spectrum
% and characterizes it.
%
% all(:,1)   = exact mass location of peak (a.m.u.)
% all(:,2:3) = peak height and uncertainty (V/Hz)
% all(:,4:5) = area under peak and uncertainty (V)

i=find(xm>=xml & xm<=xmh); % Indices in the mass range.
[y,j]=max(f(i));           % Index of the peak.
for a=1:500                          % This routine seeks
   if f(j-1+i(1)-a)<=y/2             % out the full width
      fwhml=xf(j-1+i(1)-a);          % half max of the
      break                          % peak determining
   end                               % the uncertainty in
end                                  % the frequency and
for a=1:500                          % hence the
   if f(j-1+i(1)+a)< y/2             % uncertainty in
      fwhmr=xf(j-1+i(1)+a);          % the mass.
      break                          %
   end                               %
end                                  %
dxf=(fwhmr-fwhml)/2;                 %
ind1=j-2+i(1);             % Indices of the three points
ind2=j-1+i(1);             % at the tip of the peak.
ind3=j+i(1);               %
xfstep=xf(100)-xf(99);                % Frequency step size.
temp1=max(xf(ind1:ind3))\xf(ind1:ind3);   % Normalized set
temp2=max(xm(ind1:ind3))\xm(ind1:ind3);   % of three tip
temp3=max(f(ind1:ind3))\f(ind1:ind3);     % points.
fit1=polyfit(temp1,temp3',2);  % Quad. fit in freq. domain.
fit2=polyfit(temp2,temp3',2);  % Quad. fit in mass domain.
xfmax=max(xf(ind1:ind3))*      % Frequency of peak.
      (-fit1(2)/(2*fit1(1)));  %
k=find(xf>xfmax-dxf & xf<xfmax+dxf); % Indices within FWHM
df1=mean(fb(k))/chgb;                % Background noise avg.
all(:,1)=max(xm(ind1:ind3))*         % Mass of peak.
         (-fit2(2)/(2*fit2(1)));     %
all(:,2)=(max(f(ind1:ind3))*         % Peak height.
         polyval(fit2,(-fit2(2)/     %
```

```
         (2*fit2(1)))))/chg-df1;     %
df2=(chg*gain(ind2))\                % Digitizer uncertainty.
    f(ind2)*(2^(-nb-1));             %
df3=(chg*gain(ind2)^2)\f(ind2)*50; % Gain uncertainty (50).
df4=(chg^2*gain(ind2))\              % Charge uncertainty (2%).
    f(ind2)*(0.02)*chg;              %
all(:,3)=df1+                        % Total peak height
         abs(df2-df3-df4);           % uncertainty.
all(:,5)=xfstep*sum(fb(k))/chg;      % Background area under
                                     % FWHM.
all(:,4)=(xfstep*sum(f(k)))/chg-all(:,5); % Area under FWHM.
```

Bibliography

1. Chang, C. P., et al. "Ion and Chemical Radical Effects on the Step Coverage of Plasma Enhanced Chemical Vapor Deposition Tetraethylorthosilicate Films," *Journal of Applied Physics*, *B67*:2119–2126 (February 1990).
2. Charles, C., et al. "Mass Spectrometric Study of Tetraethoxysilane and Tetraoxysilane-Oxygen Plasmas in a Diode Type Radio-Frequency Reactor," *Journal of Vacuum Science and Technology*, *A10*:1407–1413 (July/August 1992).
3. Chin, B. L. and E. P. van de Ven. "Plasma TEOS Process for Interlayer Dielectric Applications," *Solid State Technology*, *31*:119–122 (April 1988).
4. Comisarow, M. B. "Signal Modeling for Ion Cyclotron Resonance," *Journal of Chemical Physics*, *69*:4097–4104 (November 1978).
5. Emesh, Ismail T., et al. "Plasma-Enhanced Chemical Vapor Deposition of Silicon Dioxide Using Tetraethylorthosilicate (TEOS)," *Journal of the Electrochemical Society*, *B136*:3404–3408 (November 1989).
6. Guan, S. and R. T. McIver, Jr. "Optimal Phase Modulation in Stored Wave Form Inverse Fourier Transform Excitation for Fourier Transform Mass Spectrometry. I. Basic Algorithm," *Journal of Chemical Physics*, *92*:5841–5846 (May 1990).
7. Hills, G. W., et al. "Plasma TEOS as an Intermetal Dielectric in Two Level Metal Technology," *Solid State Technology*, *33*:127–132 (April 1990).
8. Ing, Jr., S.W. and W. Davern. "Glow Discharge Formation of Silicon Oxide and the Deposition of Silicon Oxide Thin Film Capacitors by Glow Discharge Techniques," *Journal of the Electrochemical Society*, *112*:284–288 (March 1965).
9. Kirov, K. I., et al. "Investigation of SiO2 Layers Deposited by Plasma Decomposition of Tetra-Ethoxy Silane in a planar Reactor," *Physica Status Solidi A: Applied Research*, *48*:609–614 (August 1978).
10. Kulisch, W., et al. "Plasma-Enhanced Chemical Vapour Deposition of Silicon Dioxide Using Tetraethoxysilane as Silicon Source," *Thin Solid Films*, *B174*:57–61 (July 1989).
11. Ledford, Jr., E. B., et al. "Exact Mass Measurement by Fourier Transform Mass Spectrometry," *Analytical Chemistry*, *52*:463–468 (March 1980).
12. Lide, D. R., editor. *CRC Handbook of Chemistry and Physics* (71 Edition). CRC Press Inc., 1990.
13. Mukherjee, S. P. and P. E. Evans. "The Depostion of Thin Films by the Decompostion of Tetra-Ethoxy Silane in a Radio Frequency Glow Discharge," *This Solid Films*, *14*:105–118 (December 1972).

14. Raupp, Gregory B. and Timothy S. Cale. "The Role of Oxygen Excitation and Loss in Plasma-Enhanced Deposition of Silicon Dioxide from Tetraethylorthosilicate," *Journal of Vacuum Science and Technology*, *B10*:37–45 (January 1992).

15. Riehl, K. B. Private Communication.

16. Riehl, K. B. *Collisional Detachment of Anions Using Fourier Transform Mass Spectrometry*. PhD dissertation, Air Force Institute of Technology, 1992.

17. Secrist, D. R. and J. D. Mackenzie. "Deposition of Silica Films by the Glow Discharge Technique," *Journal of the Electrochemical Society*, *113*:914–920 (September 1966).

18. Selamoglu, Nur, et al. "Silicon Oxide Deposition from Tetraethoxysilane in a Radio Frequency Downstream Reactor: Mechanisms and Step Coverage," *Journal of Vacuum Science and Technology*, *B7*:1345–1351 (November 1989).

19. Tompkins, Harland G., et al. "Desorption from Oxide Films Made by Plasma Enhanced Chemical Vapor Deposition Using Tetraethylorthosilicate," *Journal of Vacuum Science and Technology*, *B9*:2738–274 (November 1991).

20. Wetzel, R. C., et al. "Absolute Cross Sections for Electron-impact Ionization of the Rare-gas Atoms by the Fast-neutral-beam Method," *Physical Review A*, *35*:559–577 (January 1987).

Vita

Lieutenant Jeremy C. Holtgrave was born on 26 March 1968 at Beale Air Force Base, CA. He graduated from Central Community High School in Breese, IL in 1986. In May of 1990 he graduated from the University of Illinois at Urbana-Champaign with a Bachelor of Science degree in Physics and was commissioned an officer in the United States Air Force. He was assigned to the School of Engineering, Air Force Institute of Technology, in May 1991.

Permanent address: P.O. Box 133
Breese, Illinois 62230

REPORT DOCUMENTATION PAGE

Form Approved
OMB No. 0704-0188

1. AGENCY USE ONLY *(Leave blank)*	2. REPORT DATE	3. REPORT TYPE AND DATES COVERED
	December 1992	Master's Thesis

4. TITLE AND SUBTITLE
Cation Production and Reactions Induced by Electron Impact on Tetraethoxysilane

5. FUNDING NUMBERS

6. AUTHOR(S)
Jeremy C. Holtgrave, 1Lt, USAF

7. PERFORMING ORGANIZATION NAME(S) AND ADDRESS(ES)
Air Force Institute of Technology, WPAFB, OH 45433-6583

8. PERFORMING ORGANIZATION REPORT NUMBER

9. SPONSORING/MONITORING AGENCY NAME(S) AND ADDRESS(ES)
Dr. Alan Garscadden
WL/POOC-3
Wright-Patterson AFB, OH 45433

10. SPONSORING/MONITORING AGENCY REPORT NUMBER

11. SUPPLEMENTARY NOTES

12a. DISTRIBUTION/AVAILABILITY STATEMENT
Approved for public release; distribution unlimited

12b. DISTRIBUTION CODE

13. ABSTRACT *(Maximum 200 words)*

The production of cations by electron impact on tetraethoxysilane (TEOS) is studied with a Fourier Transform mass spectrometer (FTMS). The operating principles of FTMS are reviewed and the experimental approach to the mass calibration and cross-section measurement is discussed. The cross-sections for total and partial ionization of $Si(OC_2H_5)_4$ from threshold to 50 eV are measured. Also, the ion chemistry resulting from interactions between ions and neutral TEOS is examined.

14. SUBJECT TERMS
tetraethoxysilane, ionization cross-section by electron impact, ion chemistry, Fourier Transform mass spectrometry

15. NUMBER OF PAGES
99

16. PRICE CODE

17. SECURITY CLASSIFICATION OF REPORT	18. SECURITY CLASSIFICATION OF THIS PAGE	19. SECURITY CLASSIFICATION OF ABSTRACT	20. LIMITATION OF ABSTRACT
Unclassified	Unclassified	Unclassified	UL